A national laboratory of the U.S. Department of Energy
Office of Energy Efficiency & Renewable Energy

National Renewable Energy Laboratory

Innovation for Our Energy Future

Implementation of a Comprehensive On-Line Closed-Loop Diagnostic System for Roll-to-Roll Amorphous Silicon Solar Cell Production

Final Subcontract Report
23 April 2003—30 September 2006

T. Ellison
Energy Conversion Devices, Inc.
Troy, Michigan

Subcontract Report
NREL/SR-520-41560
May 2007

NREL is operated by Midwest Research Institute • Battelle Contract No. DE-AC36-99-GO10337

Subcontract Report
NREL/SR-520-41560
May 2007

Implementation of a Comprehensive On-Line Closed-Loop Diagnostic System for Roll-to-Roll Amorphous Silicon Solar Cell Production

Final Subcontract Report
23 April 2003—30 September 2006

T. Ellison
Energy Conversion Devices, Inc.
Troy, Michigan

NREL Technical Monitor: Richard Mitchell
Prepared under Subcontract No. ZDO-0-30628-11

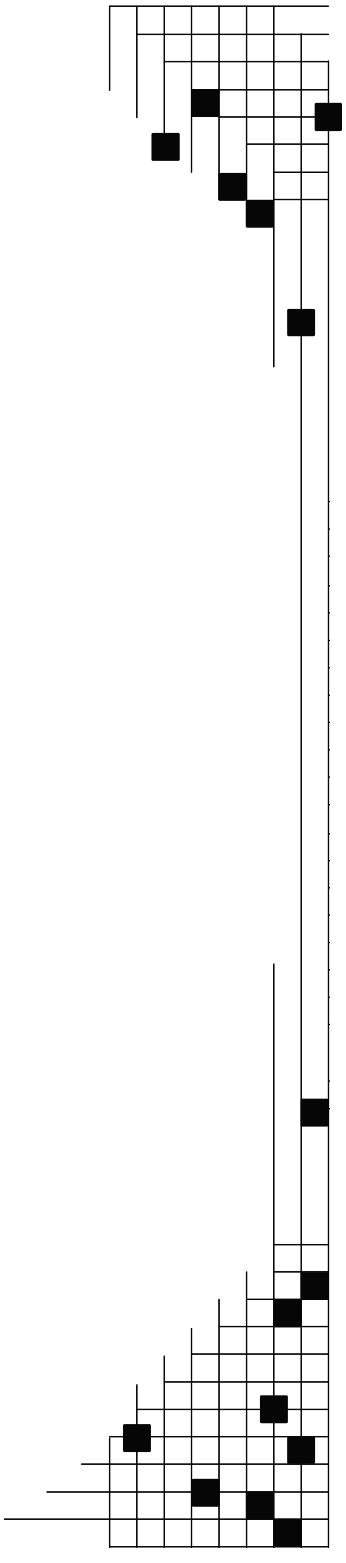

National Renewable Energy Laboratory
1617 Cole Boulevard, Golden, Colorado 80401-3393
303-275-3000 • www.nrel.gov

Operated for the U.S. Department of Energy
Office of Energy Efficiency and Renewable Energy
by Midwest Research Institute • Battelle

Contract No. DE-AC36-99-GO10337

CONTENTS

List of Figures

List of Tables

BACKGROUND AND EXECUTIVE SUMMARY

Short Summary of Accomplishments

In this program ECD has developed a comprehensive *in-situ* diagnostic system that:

- Reduces the time between deposition in the a-Si machine and device characterization from about 200 hrs to about 1 hour. These systems allow us to immediately detect significant production problems and also pin-point these problems to specific deposition zones, consequently saving up to a week of production per incident. These systems have also provided us with the capability of embarking upon a significant machine optimization program that will increase the device efficiency, and consequently product rating, and reduce product variations.
- The Photovoltaic Capacitive Diagnostic [PVCD] systems measure the open circuit voltage [V_{OC}] and Charging Rate [*CR*, a measurement of the short circuit current (I_{SC}) and intra-cell series resistance (R_S)] *for each cell* in the triple junction device prior to deposition of the top conductive oxide coating in a subsequent deposition machine. These systems operate with an rms precision of about 0.03%, and have operated for close to 4 years with no need for servicing of the electronics or for calibration. We believe that these systems, which operate with a non-phosphor solid state LED light source, have demonstrated our capability of installing high-precision diagnostic devices to expedite the commissioning of manufacturing equipment, and then operating these diagnostic devices for the lifetime of the equipment without service or calibration.
- Spectrometers are used to measure the ZnO thickness of the backreflector [BR], the a-Si thickness, and top conductive oxide, ITO, coatings. Closed loop control systems have been developed for both the ZnO and ITO deposition systems. A "Stop-and-Go On-the-Fly Static Burn" system allows us to measure the deposition rate and deposition profile of each of the more than 60 a-Si alloy deposition zones, including the very thin p- and n- doping layers.

With these systems a single individual will be able to easily monitor the operation of 10's of machines on a real-time basis; in the further future, expert systems will be able to monitor and automatically optimize 100's of machines using these diagnostic systems.

In this report we summarize the diagnostic systems developed in this program, as well as our other major accomplishments. This report concentrates on work carried out in the final [3rd] phase of this program, beginning in the Fall of 2004 and ending in the fall of 2006. This information in this report is mostly a subset of the information we have already summarized in our Monthly Reports. A summary of the previous 2 phases of this work can be found at the URL:

http://www.nrel.gov/docs/fy05osti/37660.pdf.

Note: Many of the figures in this report show "screen displays" taken from diagnostic system computer displays. Color is used extensively in these displays to convey information; consequently, some information will be lost in a black and white copy of this report. We encourage you to view the color PDF file of this report that will be made available on the NREL website.

*In particular, displays show **Bottom Cell** data in shades of red, **Middle Cell** data in shades of green, and **Top Cell** data in shades of blue – this allows one to more easily understand plots with many curves.*

Background

Energy Conversion Devices, Inc. (ECD) has developed and built 7 generations of roll-to-roll amorphous silicon PV production equipment. In the ECD/United Solar Ovonic production process we deposit an ≈ 1 μm-thick 12-layer coating consisting of a metal/oxide backreflector, a 9 layer a-Si/a-SiGe alloy triple junction solar cell, and a top transparent conductive oxide coating onto 125 μm thick, 35.5 cm wide stainless steel webs in a series of three roll-to-roll deposition machines. Figure 1 shows a schematic of the United Solar 30 MW 6-web a-Si deposition machine; a photograph of the machine is shown in Fig. 2.

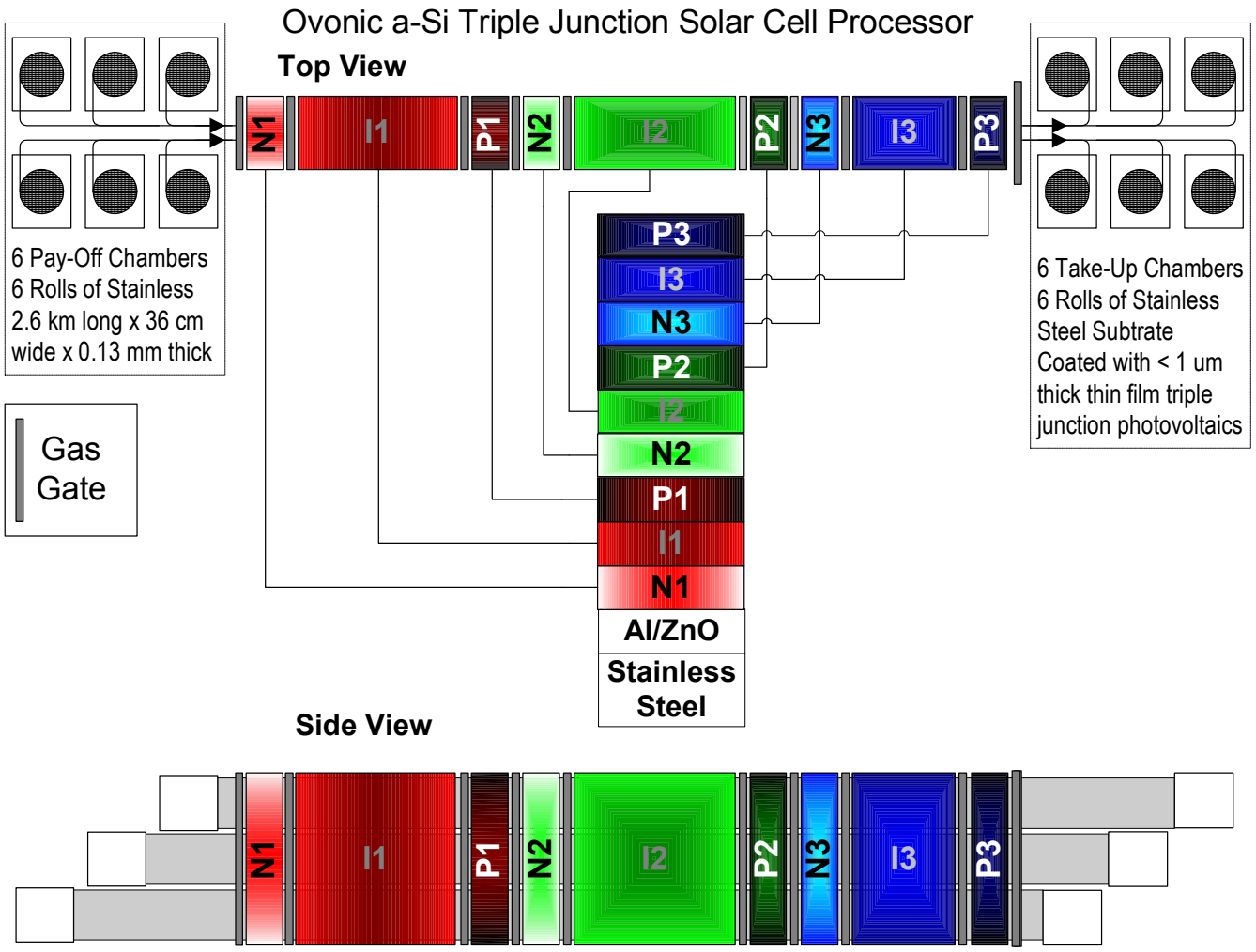

Fig. 1. Schematic of the United Solar 30 MW/yr a-Si deposition equipment.

All the developments of the previous PVMaT 5A program were incorporated into this machine:

- A substrate heating and monitoring system, using durable NiChrome heater elements;
- Reactive sputtering for low-cost deposition of the Al/ZnO backreflector;

- A new PECVD cathode that provides uniform deposition over large areas and reduced germane usage;
- "Pinch Valves" that allow the rolls of substrate to be installed and removed while keeping the deposition regions of the machine under vacuum; and
- Hardware for online diagnostic systems, including the non-contacting PV Capacitive Diagnostic (PVCD) system, which can measure the a-Si solar cell electrical properties *in-situ* without an ITO top coating, and spectrometers to measure the cell thickness.

"Included in the machine" might be an understatement: many of these technologies have been essential to the success of this machine. This machine is now serving as basis to allow us to rapidly expand our manufacturing operations, as recently announced, to:

60 MW	2006
120 MW	2007
180 MW	2008
> 300 MW	2010

Fig. 2. Side view of the United Solar 30 MW/yr a Si processor.

In this PV Manufacturing R&D Inline Diagnostics Solicitation, ECD has built upon these accomplishments to enhance the operation of the present production machine, lay the foundation for improvements in the next generation machines and has created the technology needed to operate 10's, and perhaps 100's, of machines. The four major work areas undertaken by ECD and United Solar in the present program are described below:

1. Development of closed loop thickness control systems for the ZnO, ITO layers, and a-Si component layer thicknesses (the last is an expansion of this program).
2. Continued development of the PV Capacitive Diagnostic (PVCD), in particular, the development of new "Component Cell" PVCD's for precise measurement of each of the 3 cells in the triple junction PV device.

3. The development of plasma monitoring systems to further optimize the i-layer deposition process, and for possible online implementation.
4. Yield improvements by investigating online yield measurement systems, investigations into sources of reduced yield, and mitigation of these sources.

The PV Manufacturing R&D Program has played a key roll in the incubation and development of this Roll-to-Roll manufacturing technology allowing ECD/United Solar to develop new technologies to enhance the present equipment and lay the foundation for our now rapid expansion in manufacturing capability.

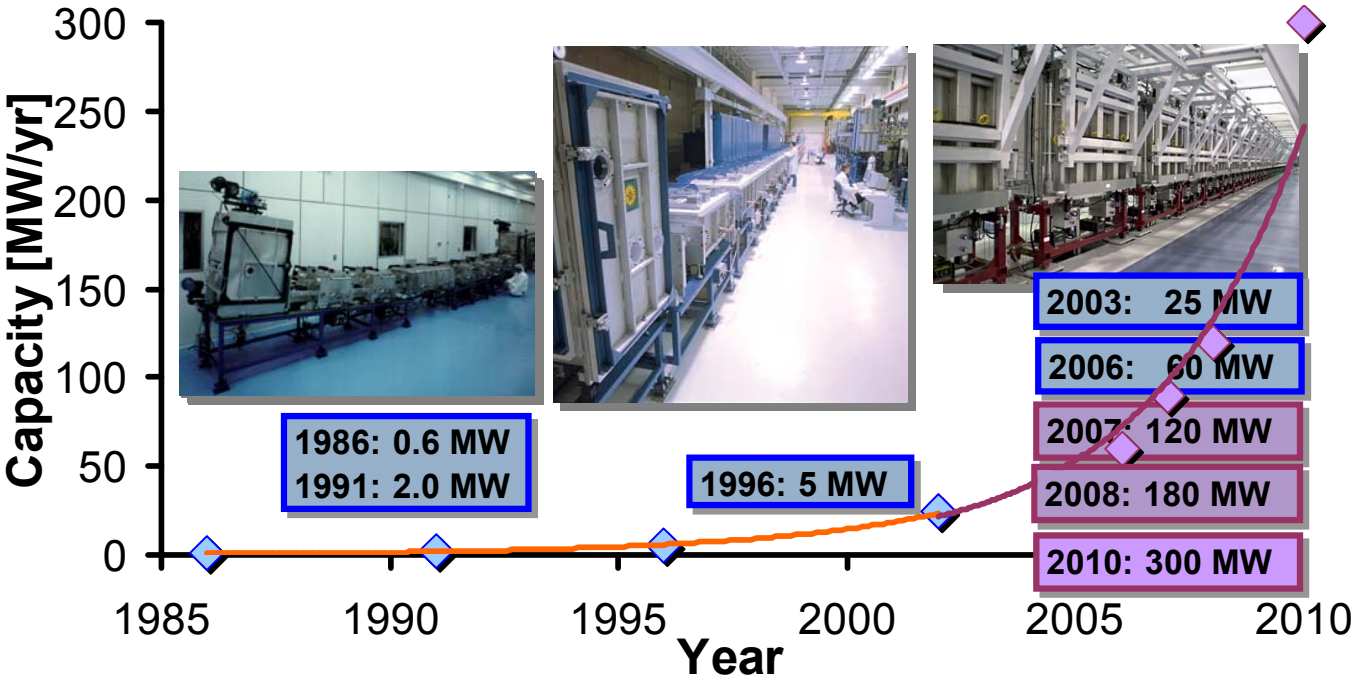

Fig. 3. ECD/United Solar Joint Venture manufacturing capacity over the last 15 years and announced plans for future expansion.

ECD has now completed the Phase III work for this program. In the following report we summarize the work in each of these tasks.

1. DEVELOPMENT OF CLOSED-LOOP CONTROL OF FILM THICKNESS

Jeff Karn (ECD), Tim Ellison, Rob Kopf, Mark Lycette (ECD);
Rujiang Liu (United Solar)**;**
David Dodge (Focus Software)

1.1 Introduction

We have successfully met, and in many areas, surpassed the goals for this work area:

- *Backreflector (BR) Machine*: We have implemented and now operate the ZnO deposition under closed loop control using a single thickness measurement system.
- *ITO Machine*: We have developed and implemented a much more complicated MIMO (Multiple Input/Multiple Output) system for control of the thickness *and cross-web uniformity* of the ITO deposition. This system will probably replace the single spectrometer system presently used for ZnO thickness control in future backreflector, BR, machines for more transversely-uniform ZnO deposition.
- *a-Si machine*: Using both the spectrometer system and the PVCD's, we developed and used a number of QA/QC techniques. The discovery and development of the "Stop-and-Go" static burn technique allows us to monitor the deposition rate and profile of each of the more than 60 deposition areas in the a-Si machine. With the present new process chamber spectrometer being developed, we see the possibility of having an expert system precisely track the deposition rate and profile for each cathode – including the very thin p-doping layers – in future machines for the ultimate in online thickness control.

Our diagnostic systems have shown us that additional diagnostic systems to monitor and control other properties of the deposited thin films (e.g., the BR texture and reflectance, and the p3-ITO tunnel junction voltage drop) can further enhance our ability improve the product efficiency and reduce variations.

1.2 3rd Generation ITO/ZnO CLTC Systems

The original operational plan for the Backreflector (BR) and ITO Deposition Machines called for measuring the film thickness at a single location along the middle web. This real-time measurement would provide the operators with the diagnostic required for tuning the machine. Further, this diagnostic would become the sensor for an automated closed loop thickness control (CLTC) system. This plan has been successfully implemented on the BR Machine where a single thickness measurement along the center web was adequate. The BR CLTC system has now been in operation for two years and has significantly minimized the need for operator intervention.

During commissioning of the ITO Machine it was found that transverse uniformity variations required an array of five spectrometers. In addition to measuring thickness, the oxygen distribution lines were outfitted with control valves to permit transverse thickness adjustment. Shown in Fig. 1.1 is the spectrometer operator display that is used for manually tuning the thickness. The top plot in this figure shows the instantaneous thickness of each of the five spectrometers while the bottom plot graphs these values over time. The step changes in the bottom plot occurred when the operator changed system settings to bring the thickness into specification.

The layout of the ITO Machine spectrometers and control points are shown schematically in Fig. 1.2. There are two Plasma Emission Monitors (PEMs) that control valves distributing oxygen to front and rear manifolds. In addition, each manifold has two valves for adjusting the cross-manifold distribution.

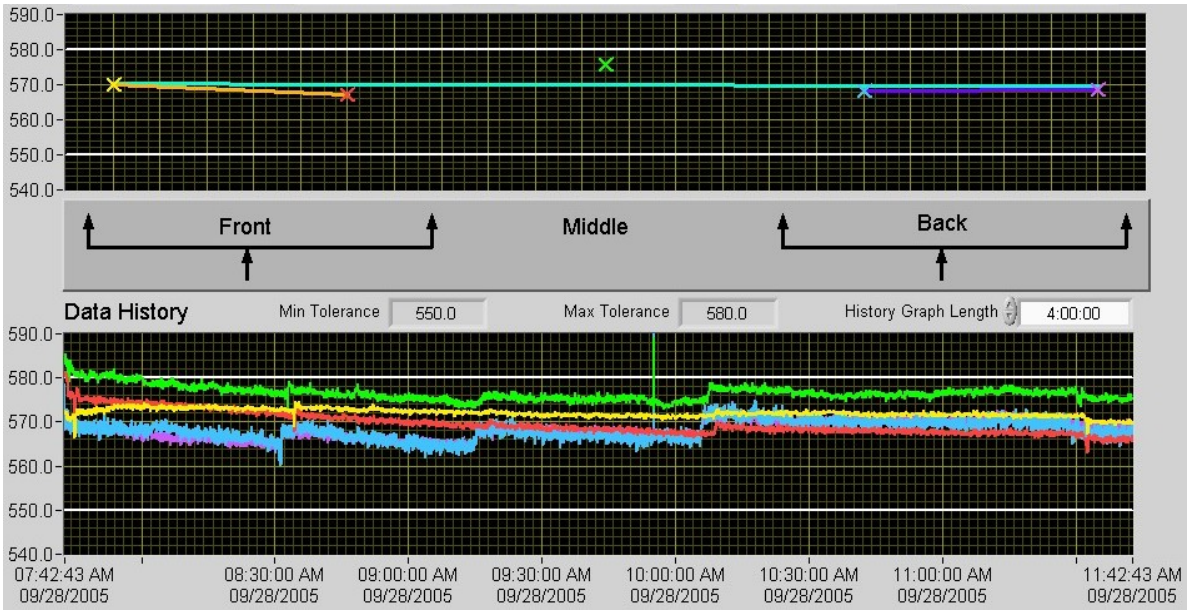

Fig. 1.1. ITO Spectrometer Operator Display. Top plot shows instantaneous thickness of all five spectrometers while the bottom plot graphs these five values over time.

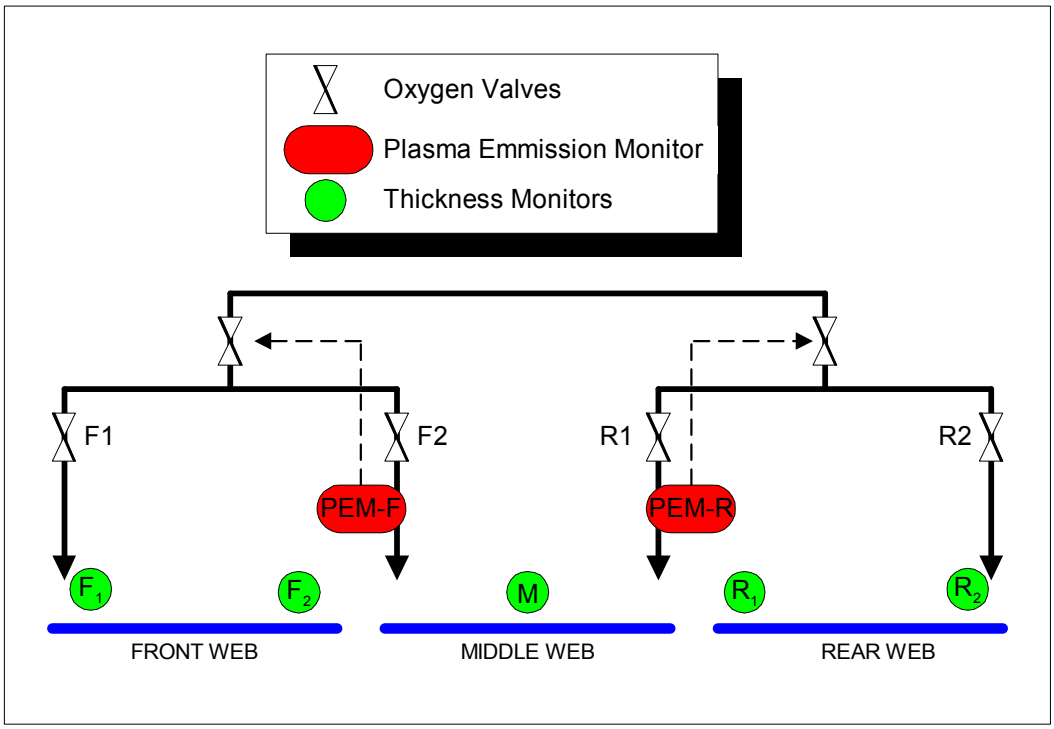

Fig. 1.2. Schematic Layout of ITO CLTC Inputs and Outputs

1.2.1 Closed Loop Thickness Control

Due to the multiple spectrometers and controls the development of the ITO CLTC system was significantly more complicated than the BR system. The ITO CLTC algorithm breaks the control process into three subsystems:

- Front Web Subsystem: Adjusts the front web uniformity by controlling the oxygen valves F1 and F2. Adjusts the overall front web thickness by changing the set-point of Plasma Emission Monitor PEM-F.
- Rear Web Subsystem: Adjusts the rear web uniformity by controlling the oxygen valves R1 and R2. Adjusts the overall rear web thickness by changing the set-point of Plasma Emission Monitor PEM-R.
- Middle Web Subsystem: No separate knob exists to adjust the middle web. Rather, the middle web thickness is controlled by coordinating the Front Web & Rear Web Subsystems.

Tuning each subsystem involves quantifying how changes to the inputs (valves and PEMs) correspond to the measured change in thickness. It was found that a single proportionality constant could be used for the Front and Rear subsystems to control the oxygen valves. Shown in Fig. 1.3 is the CLTC Expert Display. The proportionality constants for the oxygen valves and the PEM control are shown inside the red boxes of Fig. 1.3.

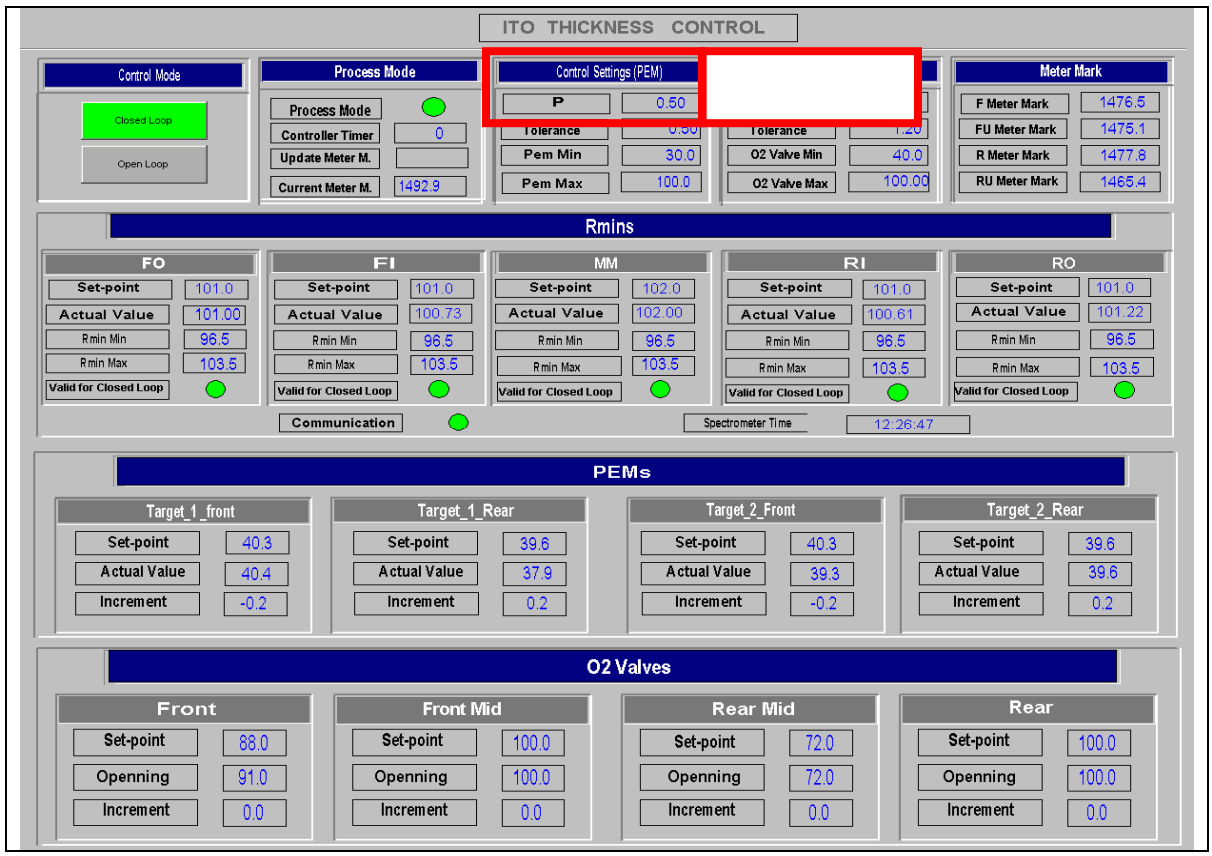

Fig. 1.3. CLTC Expert Display. Red boxes highlight the proportionality constants for the oxygen valves and PEMs.

1.2.2 Production Operation

Upon determining the proportionality constants the system was run in closed loop mode for over 600 meters of a production run. The wavelength of the ITO reflection minimum plotted over the run is shown in Fig. 1.4. Between 200 and 1400 meters, when CLTC was not running, large drifts and the occasional step-changes implemented by the operator can be seen. Between 1400 and 2100 meters the system was operating in closed loop mode. During this part of the run the drifts disappeared and the deviations between spectrometers significantly decreased. [It should be noted that the thickness in the middle continued to be an outlier. This is a limitation imposed by the gas distribution system.]

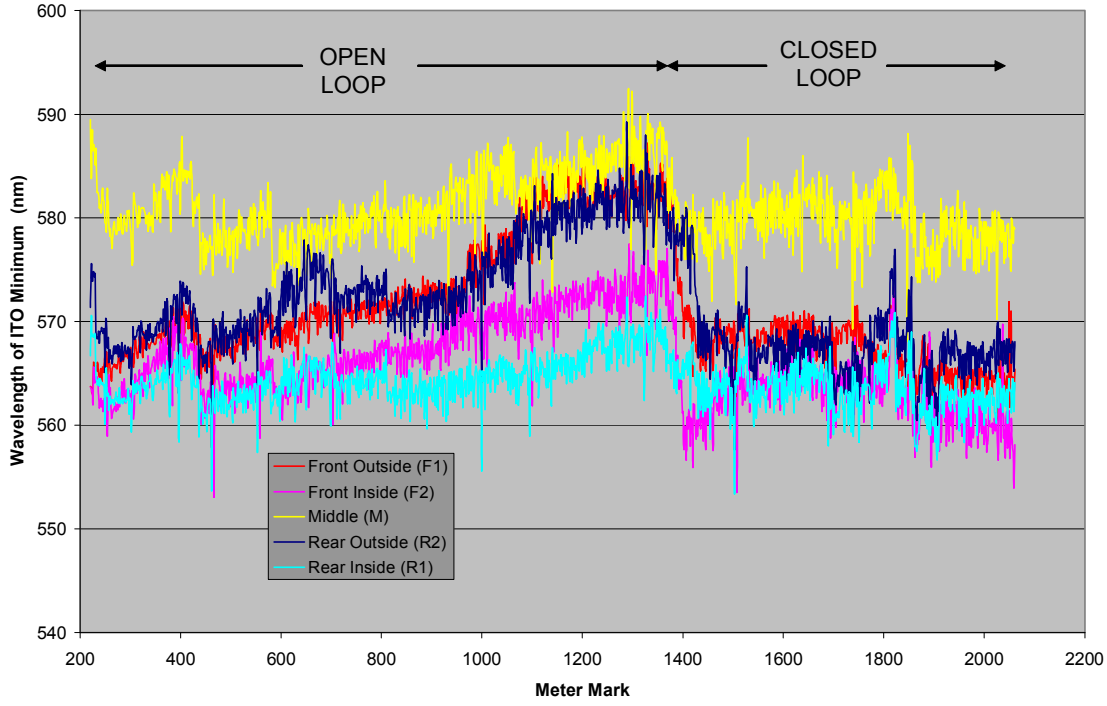

Fig. 1.4. Wavelength of the ITO Reflectance Minimum over a production run. The CLTC system began closed-loop mode at the 1400 meter mark. The resulting improvement to stability and uniformity can be seen.

1.2.3 Further Evaluation and Future Plans

While proof-of-principle has been demonstrated, full time operation of this system has been put on hold to evaluate hardware and procedural changes to the gas distribution system. These changes will require re-tuning the subsystems and determining new proportionality constants. The control software changes to accommodate the new gas manifold have been completed and are under test. The full time operation of the ITO CLTC system will be implemented soon.

1.3 a-Si Thickness and Process Control

1.3.1 Introduction

When we began this program we knew that is was important to control the thickness of the 3 cells in our triple junction device in order to maintain and optimize the device conversion efficiency, but we had little hard data documenting the degree of device thickness regulation. With the PVCD in the previous [5 MW] production machine, we were able to observe and document, online, top cell Charging Rate [*CR*] changes of ± 10%, as shown in Fig. 1.5. These changes in the top cell Charging Rate [*CR*] affected the product conversion efficiency, and were composed of ≈ 15% step changes corresponding to a single cathode plasma turning ON or OFF, and slower drifts of about the same magnitude, probably due to the build-up of a-Si flakes on the cathodes.

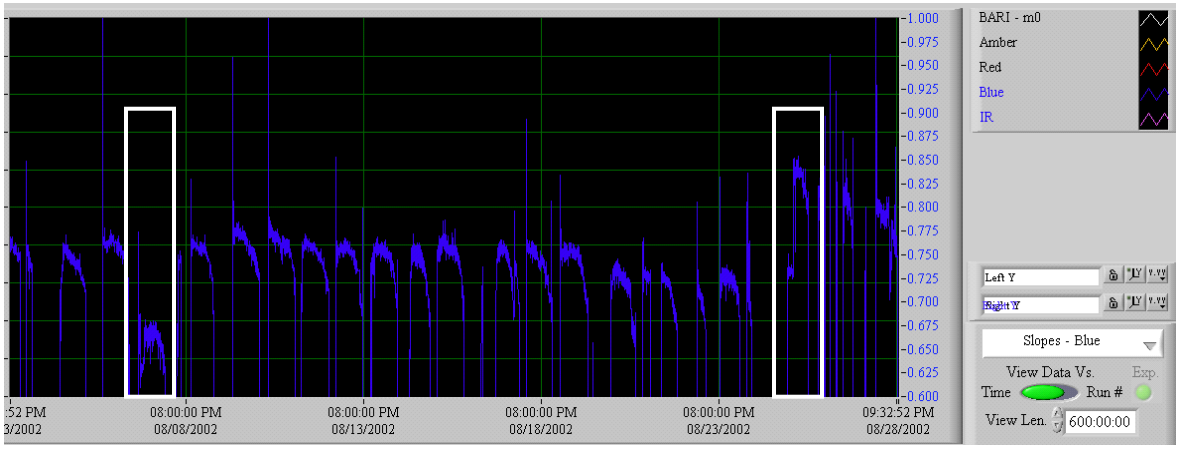

Fig. 1.5 Top Cell Charging Rate signal from the PVCD in the 5 MW production machine recorded over a 25 day period in 2002. One can observe a cathode going OFF and back ON [white boxes], as well as slow drift. The use of offline QA/QC, with its 1 -2 run delay to adjust the top cell thickness, resulted in one or several runs with a significantly non-conforming top cell thickness.

1.3.2 Long-Term Measurements in the 25 MW Equipment

The goal of this program was to implement a system to measure and control, online, the thickness of each cell in the triple junction device. We developed two tools to measure the individual cell thicknesses: the Component Cell PV Capacitive Diagnostics (PVCD's) Charging Rate [*CR*] signals and the Component Cell Reflection Spectrometers.

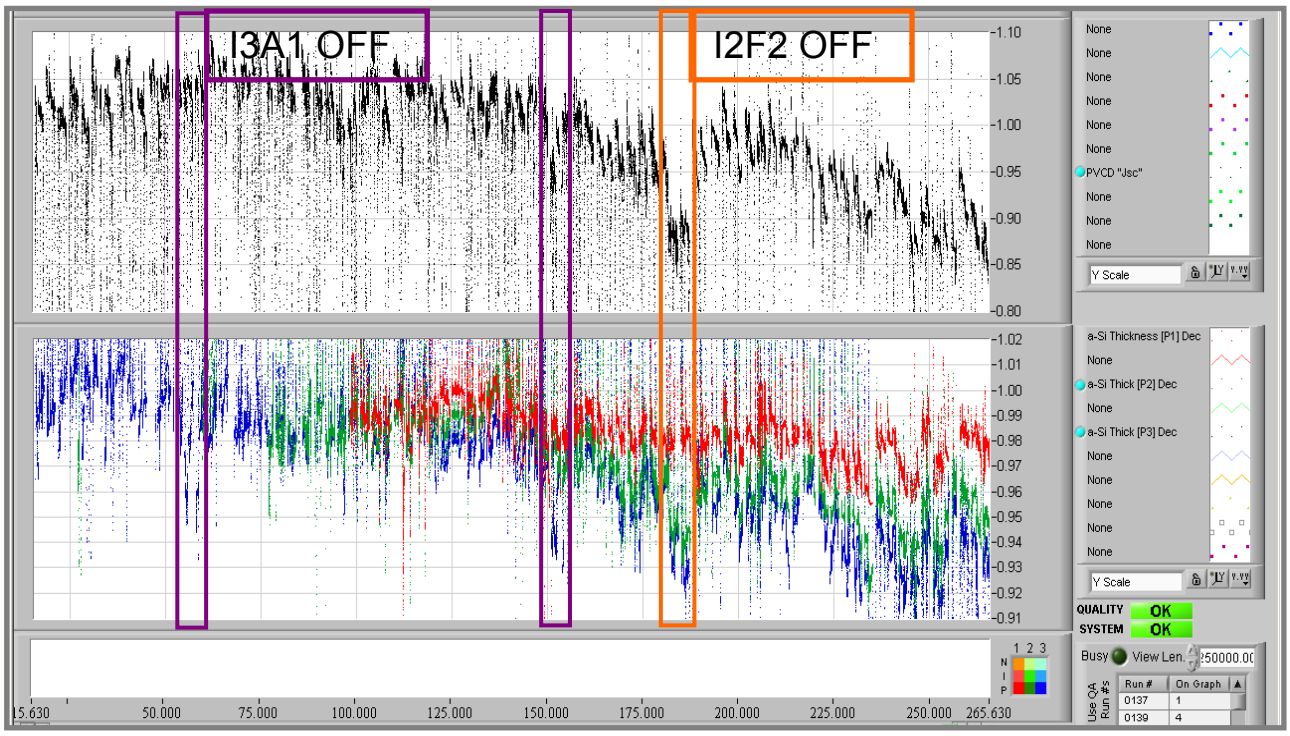

Fig. 1.6. Data Diagnostic Display (DDD) covering 250,000 m of operation showing a slow decrease in PV device charging rate signal from the PVCD [top plot, 5%/div] and correlated decrease in the relative thickness of the PV material from the **Bottom**, **Bottom + Middle**, and **Bottom + Middle + Top** cell reflection spectrometers [bottom plot, 1%/div]. Some other events causing signal variations are noted. [Horizontal: 250,000 m full scale].

Figure 1.6 shows a record of these systems in operation in the 1st 30 MW production equipment over a ¼ million meter operating period. The upper plot shows a "composite" PVCD Charging Rate, *CR*, signal (with information from all three cells), and the lower plot shows the relative thickness of the **Bottom**, **Bottom + Middle** and **Bottom + Middle + Top** cells. At the beginning of 2005, these data were telling us quite clearly that:

- The device was becoming thinner, having lost about 5% of its thickness. We knew this with high certainty since independent measurements were telling us the same story;
- The reduction in thickness was occurring in all cells; and
- From previous correlations with offline QA/QC, the reduction in thickness was reaching a critical point where efficiency would be affected.

We were most concerned about the top cell thickness, and performed an experiment in which we increased the top cell thickness as shown in Fig. 1.7. This experiment showed that the device efficiency increased as we adjusted the top cell thickness back towards its nominal value using the online diagnostic systems for feedback.

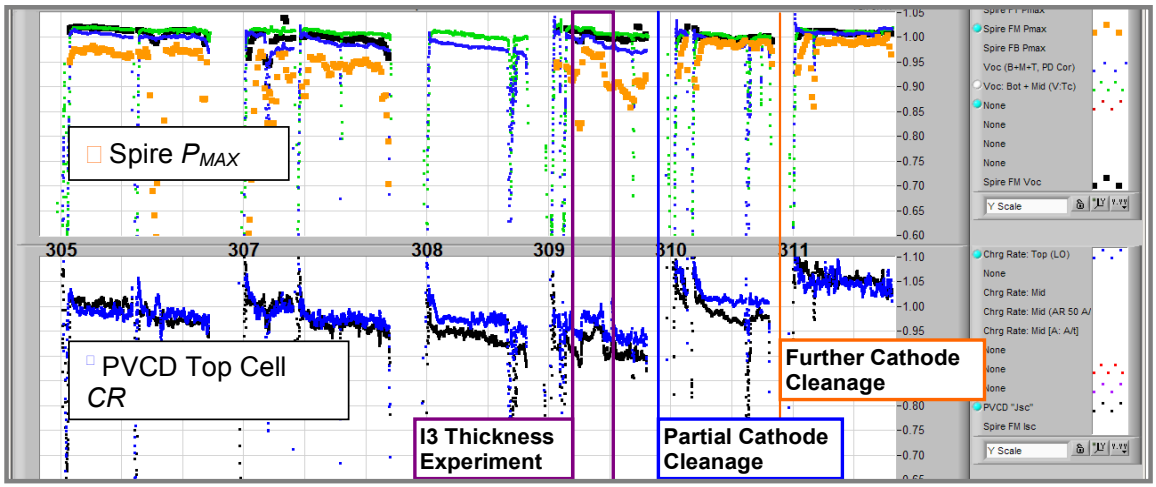

Fig. 1.7. Online and Offline data showing effect of using the online PVCD top cell CR signal to correct the cell thickness. We observed about a 5% increase in device conversion efficiency when the top cell thickness was increased.

We then performed a high resolution Static Burn, Fig. 1.8, to see whether we could learn more about the source of the cell thinning problem.

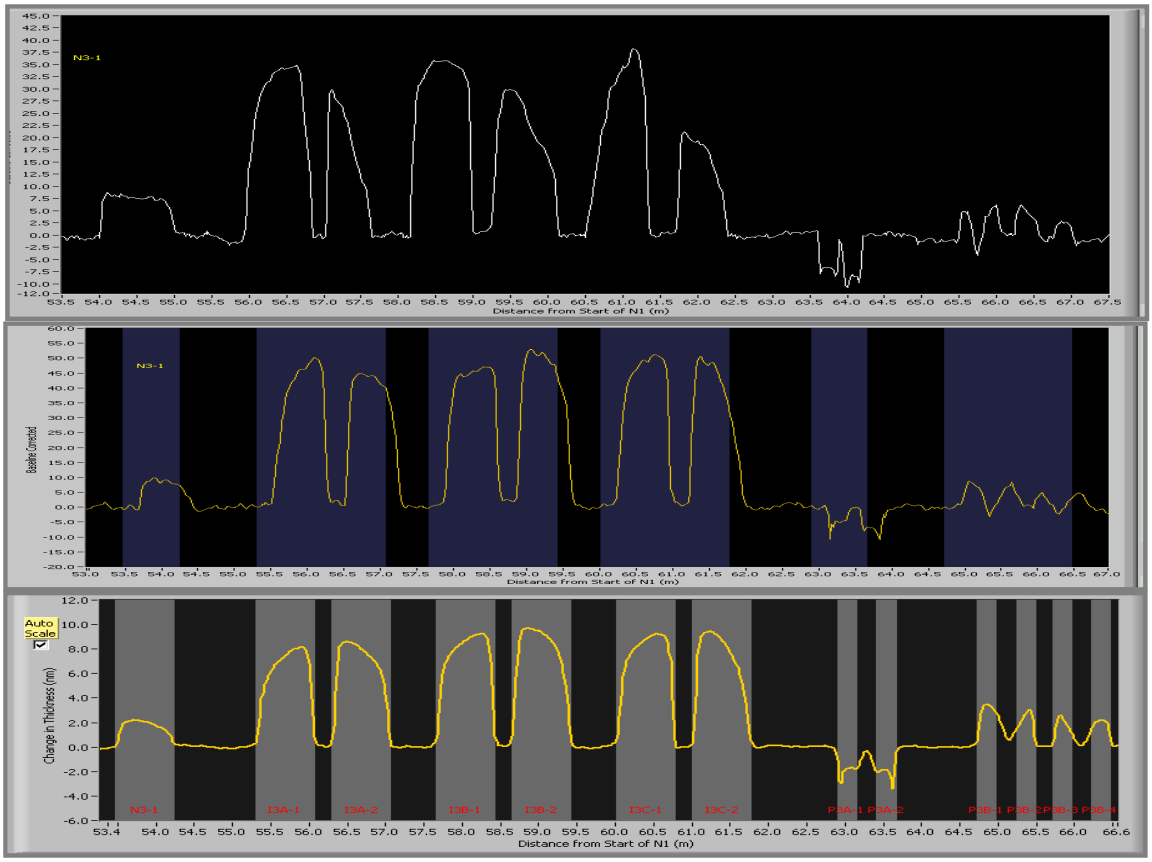

Fig. 1.8. Static Burns prior to cathode cleaning [top], after initial cleaning [middle], and standard Golden Profile [bottom].

We learned that the deposition profiles were low and distorted as shown in Fig. 1.8 (top). The Operations Group hypothesized that this may be due to a build-up of deposition on the cathodes and cleaned the cathodes. This resulted in the improved deposition profile seen in Fig. 1.8 (middle).

Figure 1.9 shows thickness and charging rate data leading up to the cathode cleanage, and for about 100 subsequent runs during which a Preventive Maintenance procedure was instituted by the USO Operations group to eliminate large deposition build-ups on the cathodes. We see that during this period the top cell charging rate stayed within about a 5% band, and then decreased by 5% when the web speed was increased by 5%. We clearly have an excellent diagnostic system with extremely good long-term stability, to monitor and stabilize the top cell thickness.

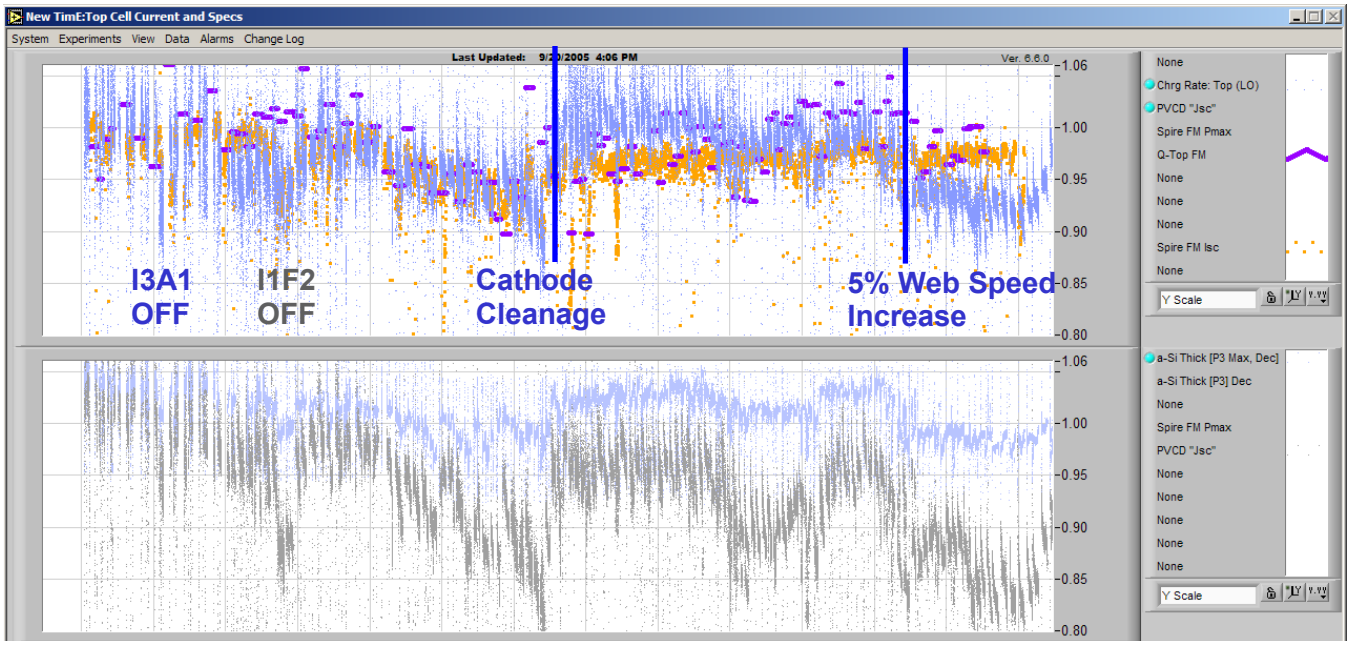

Fig. 1.9. Upper Plot: **Top Cell Charging Rage**, **Offline Spire I_{SC}**, and **Top Cell Quantum Efficiency Measurements**; Lower Plot: **Reflection Spectrometer Complete Device Thickness**, and **PVCD Complete Device Charging Rate**.

1.3.3 Short-Term Quality Control (QC) using the PVCD CR Measurement

The thickness measuring devices have also been used for online Quality Control (QC), as demonstrated in Fig. 1.10.

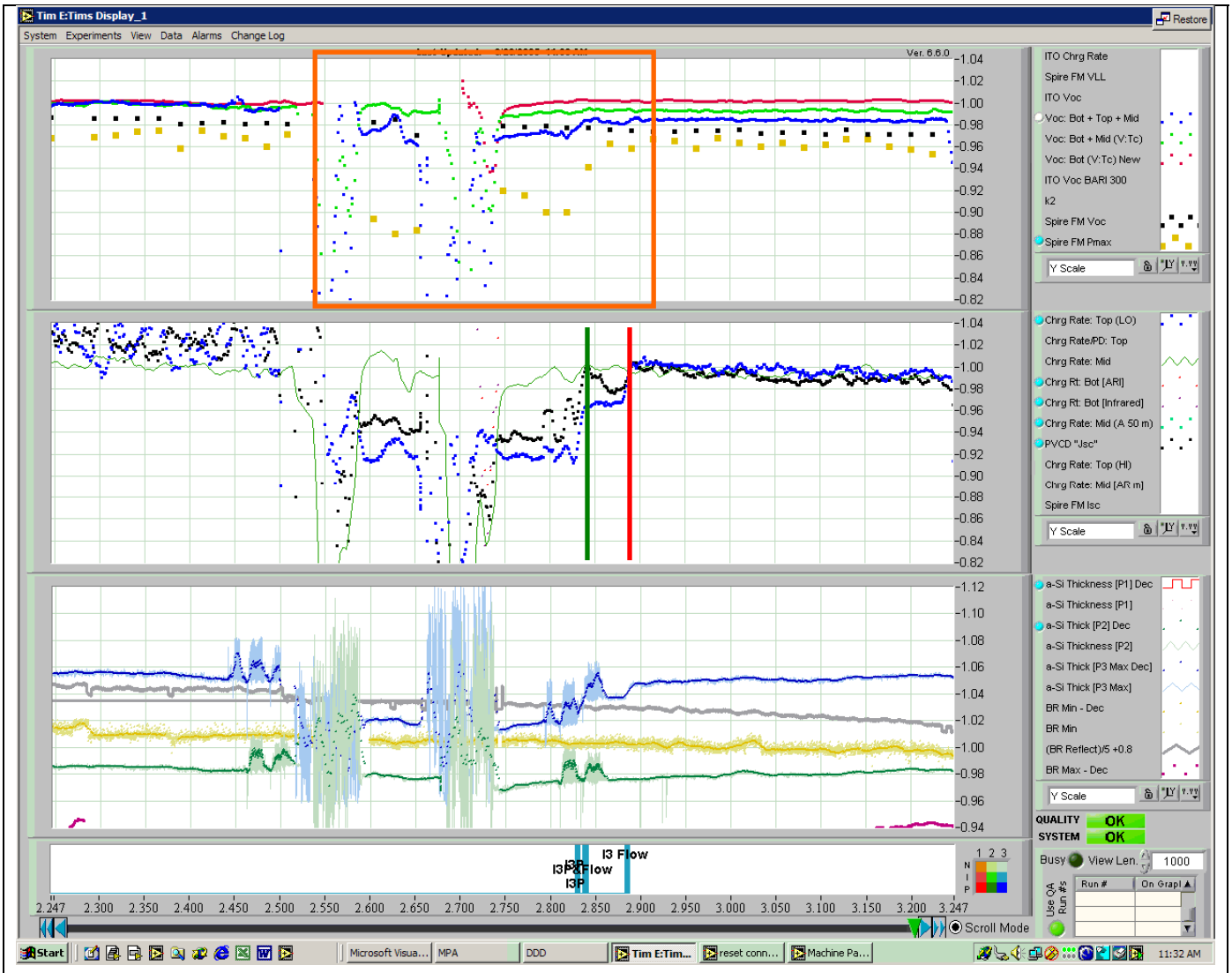

Fig. 1.10. **Upper Plot:** PVCD **Bottom**, **Bottom + Middle**, and **Bottom + Middle + Top** relative V_{OC}, and Offline Spire V_{OC} (□) and P_{MAX} (□).
Middle Plot: PVCD **Middle**, **Top**, and **Complete Device** Charging Rates
Bottom Plot: Reflection spectrometer **Bottom + Middle**, and **Complete Device** relative thickness.

In the Orange Boxed region, a cathode off in the top cell intrinsic region caused a reduction in the top cell charging rate, and the device thickness. At the **Green Vertical Bar**, a correction was made to compensate for the missing cathode; using feedback from the PVCD, a second correction was made at the **Red Vertical Bar**. In the top plot one can see the effect this correction had on the device efficiency (P_{MAX}).

1.3.4 Conclusion and Future Work

We have demonstrated – over the course of a number of years now – the ability to measure the charging rate and thickness of the PV device with good precision and a high degree of long-term stability. The systems have been used both to correct for long-term drift in the deposition conditions, and online for short-term QC to correct for deposition problems.

Our work in the future is focused in three areas:

- Increased reliability to eliminate the need for servicing (e.g. changing spectrometer light bulbs);
- Expanding our vision from thickness control to process control. Our present online systems show us that that there are variations in our product quality coming from process that are presently not under closed loop control, e.g. BR texture and reflectivity, and p3-ITO tunnel junction voltage drop; and
- Improving our static burn profilometry by the use of process chamber spectrometers to remove the baseline noise in the profiles. This will allow an expert system to precisely and quantitatively track the deposition rate and profile for each cathode in the a-Si machine, including, we think, even the very thin low p-doping regions.

1.3.4.a Increased reliability

We are carrying out further work to improve the long-term stability of the web position in the regions where we make spectrometer measurements to reduce the frequency of alignment and calibration. We shall also be looking at replacing the incandescent bulbs in these spectrometers with LED sources which should last the lifetime of the production machine.

1.3.4.b Additional process control

The online diagnostic systems have identified a number of variations in the process, affecting the product conversion efficiency, that are unrelated to the film thicknesses we are controlling, e.g.:

- The backreflector texture and reflectivity; and
- The p3-ITO tunnel junction voltage drop

1.3.4.c Improved Static Burn Signal-to-Noise

We perform two types of on-the-fly static burns:

- *A high resolution burn*, as shown in Fig. 1.8, where the web is stopped for about 3 minutes, and then restarted. This long burn results in a very good S/N profile to identify a serious production problem; the burn also creates material unusable for product.
- *A standard burn* in which the web is stopped for only 20 s. This puts a relatively small amount of additional deposition in the stack which contains 3600 s of deposition; consequently the product in not affected and no scrap is produced; on the other hand, the deposition profile is much noisier. We can use these noisier data to confirm that cathodes are operating, but we cannot not use these profiles for precise quantitative measurements; nor can these profiles resolve the thin p-layer depositions.

The S/N for the short standard burns could be much improved by making differential measurements between adjacent process-chamber spectrometers – the measured baseline noise from an upstream spectrometer can be subtracted from a downstream spectrometer measuring the baseline and added deposition from the short burn (Fig. 1.11).

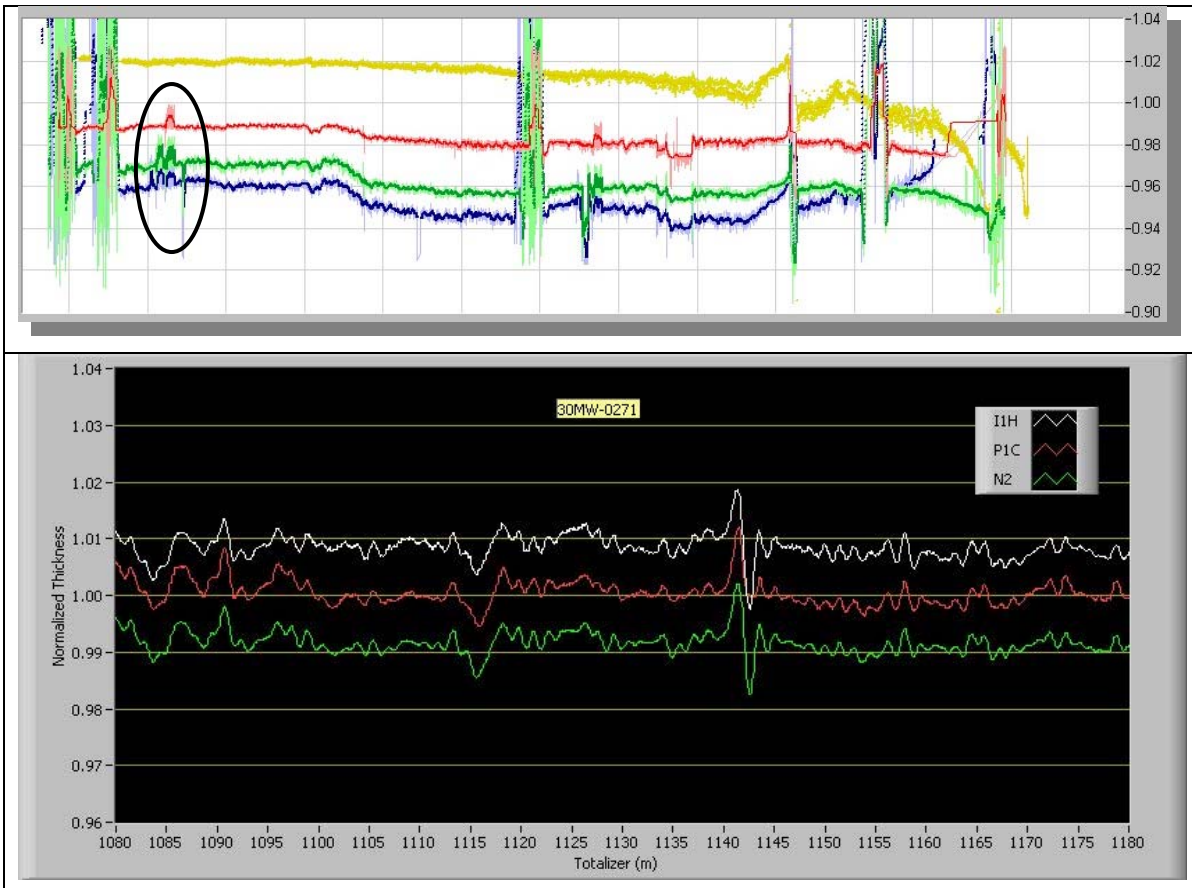

Fig. 1.11. **Top Plot**: circled region shows effect of 20 s static burn on spectrometer signals – the magnitude of the deviation is about 1%.

Bottom Plot: Spectrometer signals measured after the I1, P2, and N2 layers are deposited. Once can how the "noise" is mainly due to real thickness changes from previously deposited layers.

Key to making this work will be a very stable thickness measurement made inside a process chamber. To accomplish this we have designed, and fabricated, a spectrometer design (Fig. 1.12) which significantly reduces the distance between the spectrometer optics and the web, the single most important optical consideration, and incorporated a new web-stabilization scheme. As with the significant improvements developed for the next generation Component Cell PVCD's described in the next section, this improvement was made possible by designing the spectrometer in synergy with the the vacuum chamber to optimize the performance of the diagnostic system hardware.

With these differential measurements we believe we shall be able to use an Expert System to precisely and quantitatively track the deposition thickness and profile for each of the 60 + cathodes in the a-Si deposition machine – the ultimate in online QA/QC.

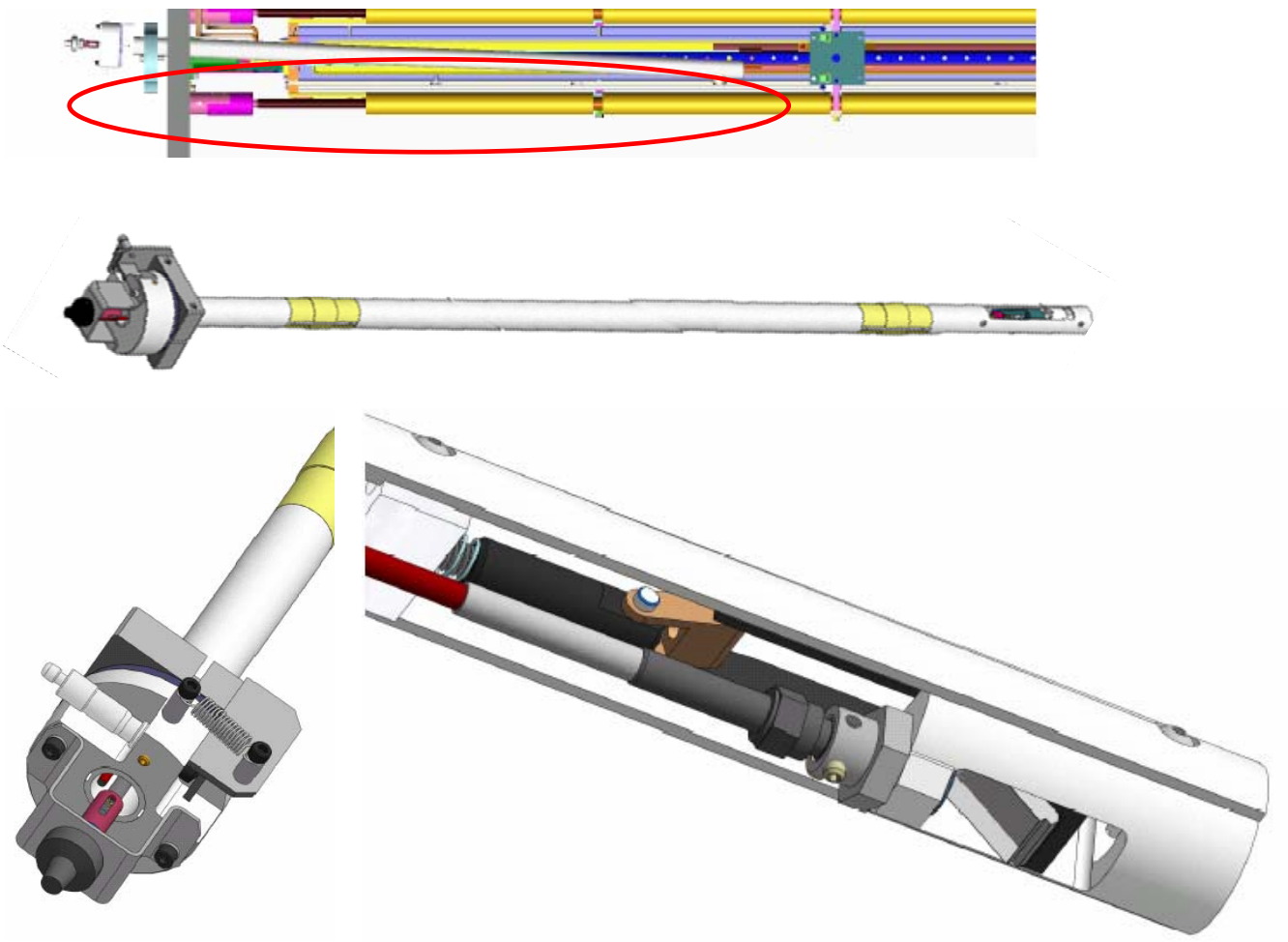

Fig. 1.12. New Mark Lycette design for *in-situ* process chamber spectrometer. Top: installation showing how the device is angled to position the optics as close as possible to the web; Middle: inside alignment fixture; Bottom: close up the business ends: left: alignment adjustment mechanism; right: final remote optics adjustments. The design geometry eliminates reflections from the window.

2. COMPONENT CELL PV CAPACITIVE DIAGNOSTIC (PVCD) DESIGN AND FABRICATION FOR BOTTOM AND MIDDLE CELLS

– Tim Ellison, Rob Kopf, Jeff Karn and Wayne Messing (ECD)
Dave Dodge (Focus Software)

2.1 Introduction and Background

In the PVMaT 5A program we developed the PV Capacitive Diagnostic (PVCD) [1]. This device has proven its capability to make precise (≈ 0.05%) in-line measurements [2,3] of the PV device open circuit voltage, V_{OC}, and short circuit current divided by cell capacity, J_{SC}/C. The PVCD also provides information on the cell series resistance, R_S. This non-contacting device works on material both before and after application of the top ITO coating, and has become an essential online diagnostic for production QA.

The goal of this program was to extend this technology to be able to characterize *each component cell* of the triple-junction device. While the original PVCD could precisely measure the triple-junction device V_{OC}, it could not unambiguously tell us which of the three cells had changed. We envisioned a series of three PVCD's, one following each completed cell.

The original PVCD was developed to operate in the Take-Up chamber of the a-Si machine. This task was "simple" in that in the Take-Up chamber:

- There are few space constraints;
- The device is far from any EMI-generating plasmas and heaters;
- The device can easily be shielded from extraneous light and ionized gas generated by plasmas;
- The device design did not require the use of ultra-high purity vacuum materials and techniques necessary to install the device inside the deposition part of the machine.
- The device was easily accessible for service, modifications, and calibration.

The Component Cell PVCD developed in this program had all these additional constraints – and it was not clear whether it could even be made to operate in such an environment.

The Component Cell PVCD's are now operating for both the Bottom and Middle cells as precision online Quality Assurance (QA) tools that allow us to measure the open circuit voltage, V_{OC}, and charging rate, CR, online, for each cell in the triple junction device.

---

[1] Tim Ellison, "Non-contacting PV Capacitive Diagnostic (PVCD) System for real-time in-situ analysis, QA/QC, and optimization", *Proc. 28th IEEE Photovoltaic Specialists Conference* (Anchorage Alaska, 15 – 22 Sept 2000).

[2] Greg DeMaggio et al., "Development of Online Diagnostic Systems for Roll-to-Roll a-Si Production: ECD's PV Manufacturing R&D Program", Proceedings of the 2003 NCPV Review Meeting (Denver, 24 – 26 March 2003).

[3] Masat Izu and Tim Ellison, "Roll-to-roll manufacturing of amorphous silicon alloy solar cells with in-situ cell performance diagnostics" in Solar Energy Materials and Solar Cells, Elsevier Science B.V., Amsterdam.

The PV Capacitive Diagnostic (PVCD) measurement system has a number of features that enable it to assist and carry out optimization activities including:

- *Precision* – the measured standard deviation for PVCD open circuit voltage, V_{OC} and charging rate, *CR*, measurements is about 0.04% - 0.05%; consequently the PVCD system can resolve very small changes in device performance, undetectable in offline QA/QC, as process conditions are varied .
- *Spatial Resolution* – the systems presently sample the web about every 1- 2 m – more than an order of magnitude higher spatial resolution than offline QA/QC measurements which enables a much higher throughput and bandwidth for continuous automated optimization. With a slight decrease in signal to noise we could increase the bandwidth of these devices to measure each cell (0.25 m resolution).
- *High Feedback Rate* – the online PVCD systems decrease the delay between deposition and characterization by more than a factor of 100 – from on the order of a week to the order of an hour.
- *Long Term Stability and Reliability* – To ensure reliability, the devices have built-in diagnostics and calibration systems:
  -- An online system measures the calibration of the entire electronics system every few minutes with a precision of 0.01%.
  -- There are also other system-diagnostics, such as a continuous measurement of the substrate temperature, data-logging of the LED light source current, and measurement of the light pulse amplitude.

  The PVCD systems have operated for over 3 years without need for calibration or replacement of any electronics. By contrast, a DC simulator must have its bulb changed on about a monthly basis which requiring recalibration, in addition to changes in calibration throughout the month. This exceptional degree of long term stability is a result of the stable geometry and the use of phosphor-less solid state (LED) light sources. We are now seeing the possibility of installing these systems to expedite commissioning and then operate for the lifetime of the machine without need for re-calibration or major service – essential attributes for diagnostic systems as ECD expands United Solar Ovonic's manufacturing capacity from a single machine today to about 10 machines by 2010, and perhaps 75 machines by 2015. We are also looking at expanding this LED light source capability to our spectrometer systems.

These systems make online troubleshooting much easier – rather than saying we have a problem, we are now invariably able to quickly pinpoint problems to specific cathodes, online, and adjust the process online to compensate. Even in offline QA/QC testing, we only obtain a V_{OC} for the complete device; online we now have precise information on the V_{OC} for each of the component cells.

The first generation Component Cell PVCD developed in this program, shown in Fig. 2.1, is still in operation in the first United Solar Ovonics (USO) 30 MW production equipment. Based upon experience with these first generation experimental systems, a second generation system, Fig. 2.2-3, has been designed and fabricated for the second and future 30 MW production machines. Mark Lycette envisioned and modeled a new "Atrium Geometry" PVCD with many advantages. The PVCD system was designed in harmony with a new larger diagnostic chamber. This synergistic design allowed him to incorporate many improvements and overcome numerous design challenges. Enhancements include:

- Removal of ***all*** the electronics and delicate electrical feed-thru's from vacuum;
- Elimination of inside-the-vacuum water cooling and argon purging of the PVCD head and electronics (e.g. LED light source, photo-detectors, etc.);
- Elimination of inside-the-vacuum water cooling for the pusher plate;
- Provisions to access the PVCD head and all electronics without breaking vacuum;
- Increased serviceability.

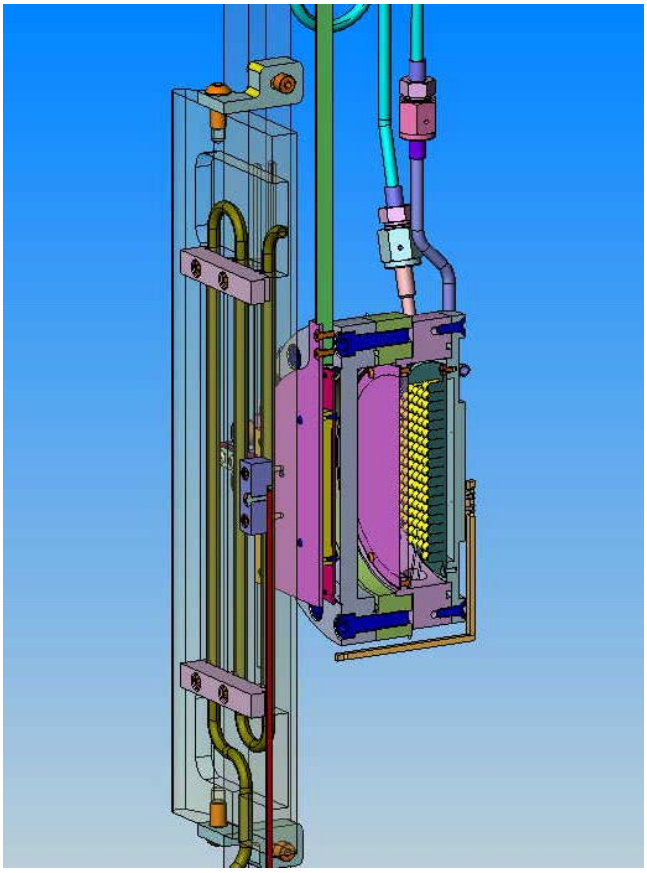

Fig. 2.1. Close-up view section view of the PVCD sensor head, shutter, and transparent view of the "pusher plate".

This design also minimizes, or eliminates, risk: the new system is all outside the vacuum – the PVCD head can be removed during operation, and a simple component-to-cover plate swap returns the configuration to an empty diagnostic chamber.

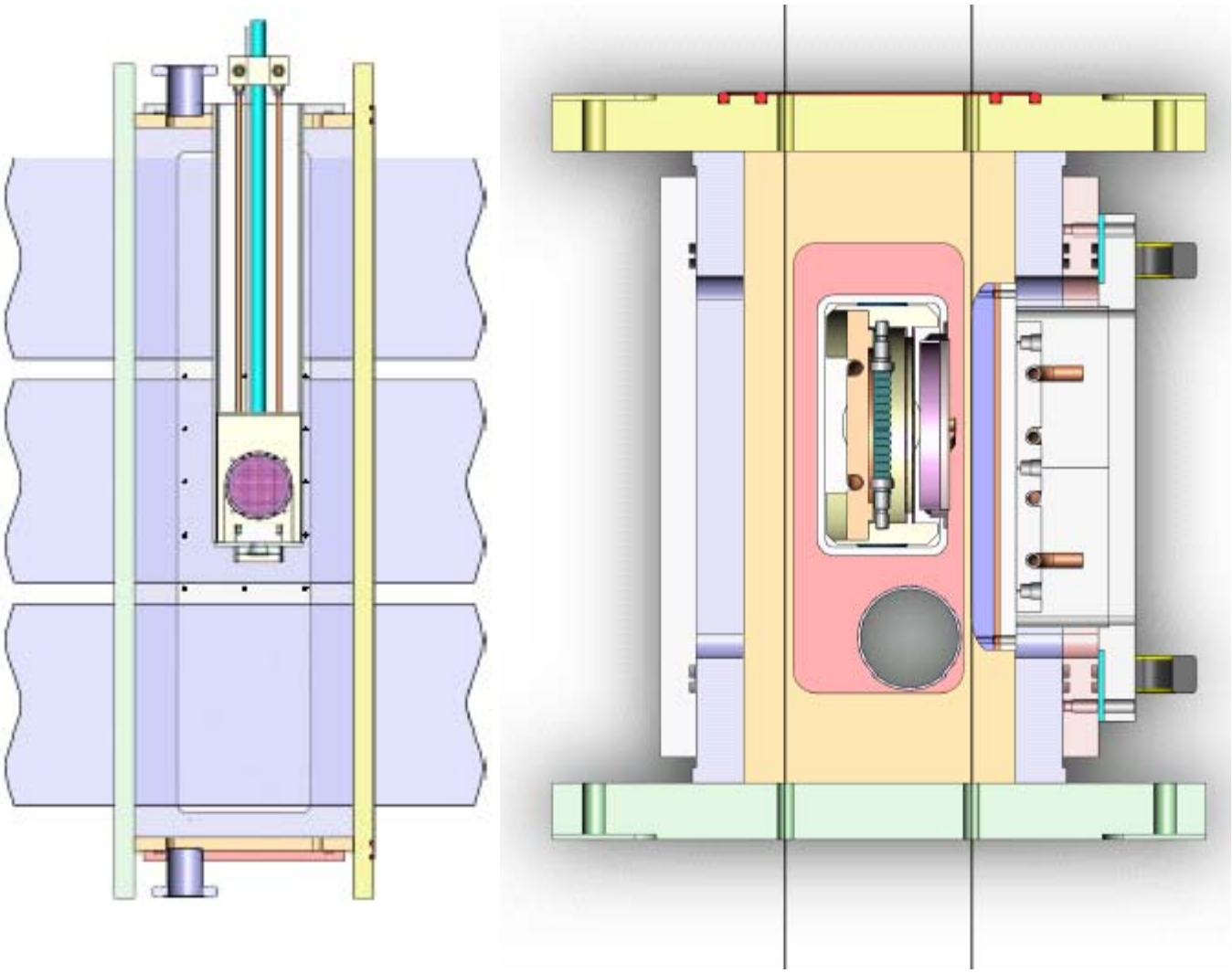

Figs. 2.2-3. Side and top sections showing the new Mark Lycette “Atrium Design” Component Cell PVCD.

In the following 3 sections we highlight a few examples of how the PVCD system can be used for online QA/QC by looking at the system from three different perspectives:

- Past usage for optimization, and Quality Control (QC), and problem diagnosis;
- Near term future uses for added QC; and
- Longer term QC from the perspective of operating 10 to 100 production machines with small core QA/QC and optimization group.

2.2. Uses of the PVCD System for Online QA/QC

2.2.1 Past Uses of the PVCD System for Quality Assurance and Quality Control [QA/QC]

In the past few years we have used these experimental/developmental devices to:

- *Diagnose severe problems and stop runs for repair*: This system has several times detected significant process problems, and pinpointed to source of the problem to a specific cathode in the 60+ cathode a-Si deposition machine. In each case, the run was stopped, avoiding long runs making scrap material, with the problem diagnosed. A single severe un-diagnosed production problem in a single a-Si deposition machine can cost United Solar 1 - 2 million dollars in lost sales.
- *Diagnose problems and correct problems on-the-fly during a run*. We have also used the PVCD system to diagnose and correct problems on-the-fly.
- *Diagnose and correct long-term drift problems prior to their becoming critical*. The long-term stability and high precision of the PVCD systems allow us to observe, and correct, long-term drift problems before they can be detected with offline QA/QC and before they become critical.
- *Optimize the process to increase the product efficiency*. The high precision of the PVCD system allows us to detect small variations in product characteristics with small variations in process inputs, allowing us to optimize the process. Every percent increase in efficiency leads to about 1 M$/year/machine increased profits when incorporated into a product rating change.
- *Diagnose source of product variation.* The PVCD system can detect small product variations due to small changes in the process, allowing us to determine the source of the variation.

2.2.1.a Diagnosis of severe problems – "Saved Runs"

The most easily documented cost savings result from the use of the online diagnostic systems to stop a 400 kW-batch run at the beginning, with a problem not only identified, but also diagnosed to a specific chamber or cathode. In such a situation we not only save the current run, but subsequent runs and the time that would be spent trying to diagnose the source of the problem offline. We have identified cathode outages in doping regions and water leaks.

Below we show an example of how the PVCD system recognized a critical process problem in the a-Si production machine and initiated a process stop after pinpointing the problem to a specific cathode. At the beginning of the run the PVCD open circuit voltages, V_{OC}, were low for the **Bottom + Middle** and **Bottom + Middle + Top** Cell PVCD's causing an alarm. Since there was no V_{OC} problem detected by the **Bottom Component Cell** PVCD, the data clearly showed that the problem originated in the middle cell. A subsequent "Stop-and-Go" static burn using the spectrometer system pinpointed the problem to the n-2 cathode. The machine was stopped and the problem corrected.

Perhaps one of the most important features of this Run Stoppage was the fact that at the time this problem occurred, the principal diagnostic system expert was out of town at NREL. The problem was correctly recognized and diagnosed by the production staff using the tools that we developed in this program.

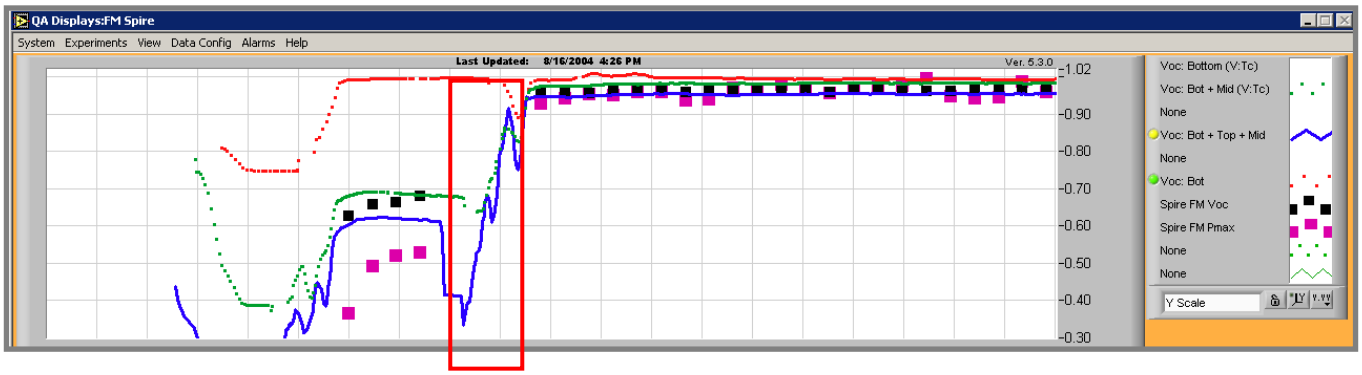

Fig. 2.4. DDD screen capture showing the effect of the n-2 cathode outage on the online open circuit voltage measurement made by the **Bottom Component Cell PVCD**, **Bottom + Middle Component Cell PVCD**, and **Bottom + Middle + Top Component Cell PVCD**. Also shown are the offline Spire V_{OC} [□] and P_{MAX} [□] measurements. The red rectangular box shows where the production run was stopped and re-started. [Vertical: 10%/div; Horizontal: 1000 m full scale].

2.2.1.b On-the-Fly problem detection and correction

In section 1.3.3, in discussing closed loop thickness control in the a-Si machine, we showed and example of how the PVCD and spectrometer systems had been used to detect, pinpoint, and correct for a cathode outage in the I3 region without stopping a run.

2.2.1.c Recognition and correction of long-term drift

In section 1.3.2, in discussing closed loop thickness control in the a-Si machine, we showed and example of how the PVCD and spectrometer systems had been used to detect, pinpoint, and correct for a long-term drift problem in the I3 deposition rate.

2.2.1.d Optimize the process to increase the product efficiency.

The high precision of the PVCD system allows us to detect small variations in product characteristics with small variations in process inputs, allowing us to optimize the process. Every 1% percent increase in efficiency leads to about 1 M$/year/machine increased profits when incorporated into a product rating change. Below we show an example of how the PVCD system was used to identify a specific change in the process that lead to improved product conversion efficiency.

Very small perturbation experiments, which were not observed in offline QA/QC, indicated that the device current and voltage could be increased by increasing the thickness of the n3 layer. Figure 1 shows subsequent experiments making large variations in the n3 layer and the corresponding increase in the product P_{MAX} ([□], top plot Fig. 1) as measured by offline QA/QC.

At the beginning of the run we also see another example of an “on-the-fly” correction to correct the top cell charging rate that lead to about a 7% increase in product efficiency [Black vertical line, Fig. 2.5].

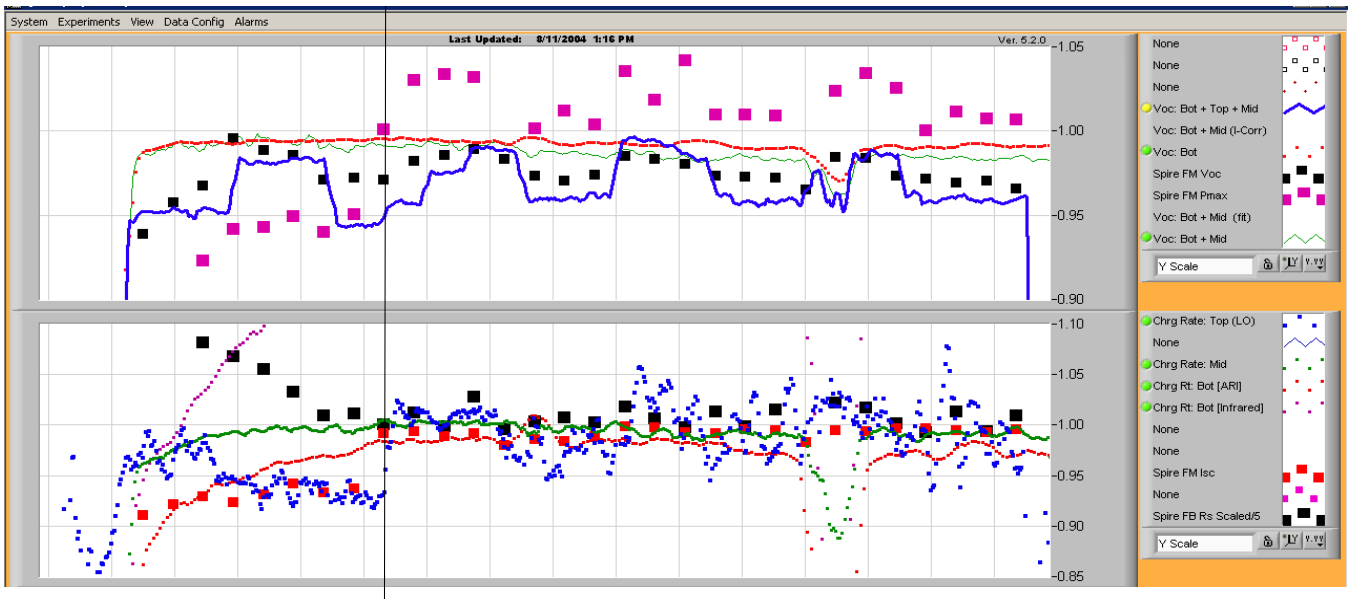

Fig. 2.5. DDD screen capture showing the on-the-fly correction of a PVCD-detected I3 cathode outage and the resulting improvement in product, and n3 thickness modulation experiments – we we a couple of percent increase in P_{MAX} [□] with increased n3 thickness. [Horizontal: 800 m full scale].

2.2.1.e Diagnose sources of product variations

We provide a couple of examples that show how the PVCD system, combined with the Diagnostic Data Display, easily make clear the sources of variations in the product quality. We look at two examples: variations in the germane concentration of the Bottom and Middle cells, and variations in the reflectivity and texture of the Backreflector.

Variations in the germane concentration

Germane concentration variation causes changes in the product electrical properties, principally the bottom cell current and V_{OC}. The PVCD system clearly shows these production variations as shown in Fig. 2.6, where changes in the germane gas source are mapped on the bottom-most plot (circled in **orange**).

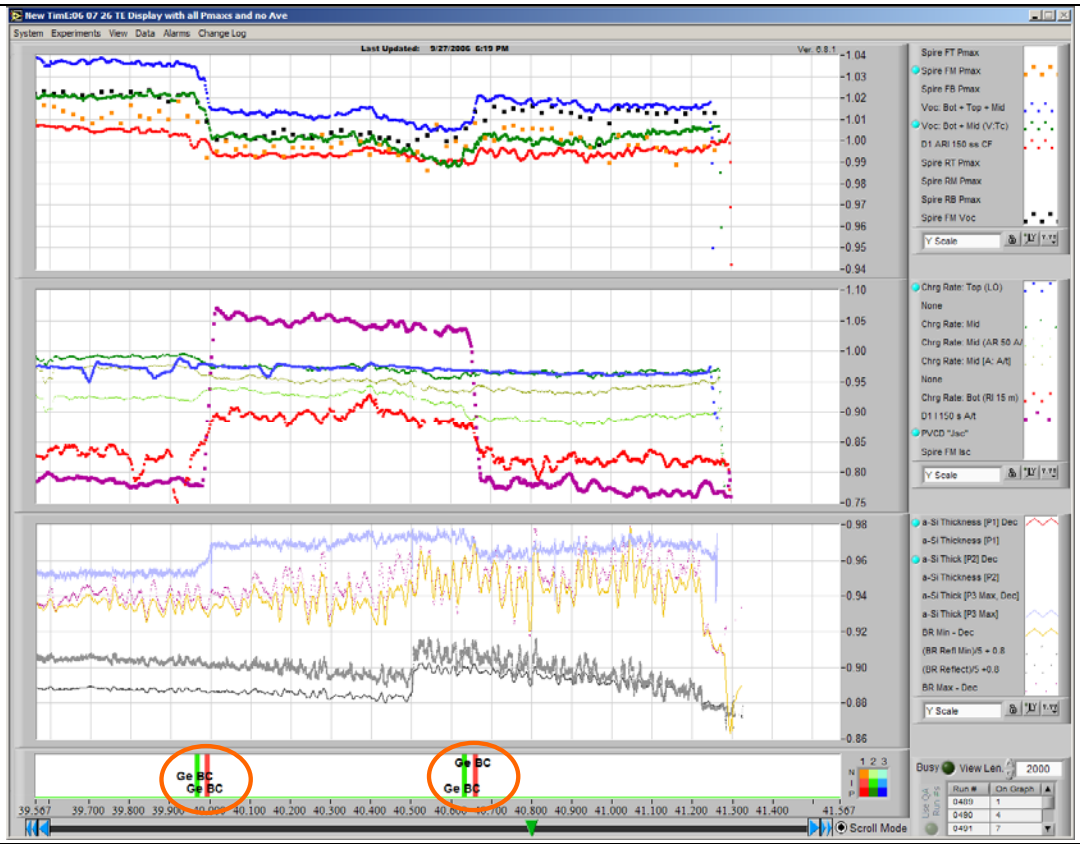

Fig. 2.6. DDD display showing online and offline device measurements which are strongly affected by the change in Germane gas source.
Top Plot: **Bottom**, **Bottom + Middle**, and **Bottom + Middle + Top** Cell V_{OC} as measured by the online PVCD system, and offline Spire V_{OC} [□] and P_{MAX} [□] measurements [Vertical: 1%/div; Horizontal: 2000 m full scale]. We observe about a 1.5% change in the product VOC and PMAX when the germane gas bottle is changed.
Middle Plot: Various Charging Rate signals from all three PVCD units; note in particular the **plum-colored trace** which shows the Charging Rate for the Bottom Cell when illuminated with an infrared light source [5%/div]. This signal was developed and is displayed to provide a highly-leveraged signal to monitor the device germane content.

Backreflector Reflectance and Texture Variations

Figure 2.7 clearly shows that nearly all the variations in the device V_{OC} are a consequence of the changes in the V_{OC} of the Bottom and Middle cells – and the vast majority of these variations originate in the Bottom cell as shown in Fig. 2.8.

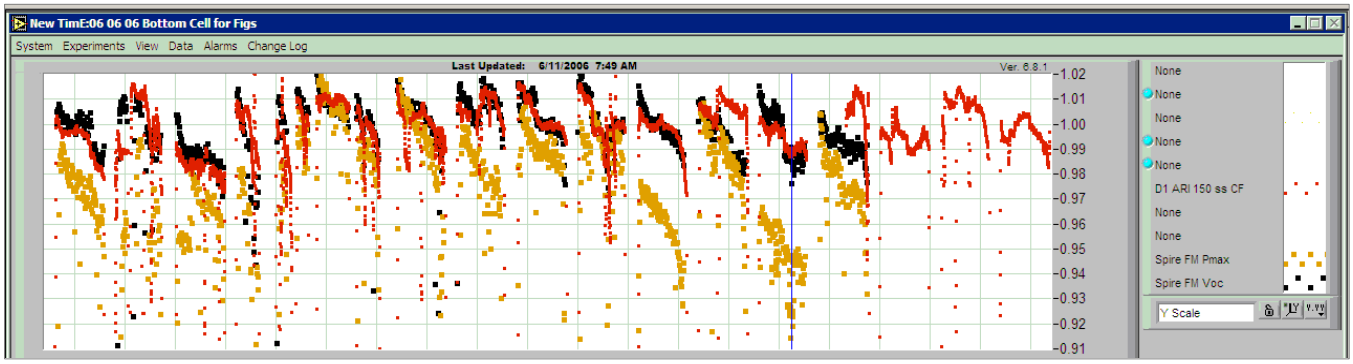

Fig. 2.7. DDD* display showing the United Solar product relative open circuit voltage, V_{OC}, as measured by offline QA/QC [■] and online Bottom + Middle Component Cell PV Capacitive Diagnostic* [ ] over twenty 2500 m runs [Veritcal: 1%/div; Horizontal: 60 km full scale]. This figure demonstrates the accuracy and precision of the PVCD device, as well as its ability to diagnose variations in product performance: from this plot we can see that nearly all variations occur prior to deposition of the top cell; additional diagnostics from the Bottom Component Cell PVCD allowed determination of the sources of these variations. The faint small orange points show the offline Spire P_{MAX} measurements.

Figure 2.8 shows is a screen capture of the online Data Diagnostics Display (DDD) showing measurements of the **Online Bottom Cell V_{OC}** and the Offline Spire triple-junction V_{OC} (■) and P_{MAX} (■). The online bottom cell V_{OC} measurements are from the Bottom Component Cell PVCD. Component V_{OC} measurements are not available in any offline QA/QC measurements.

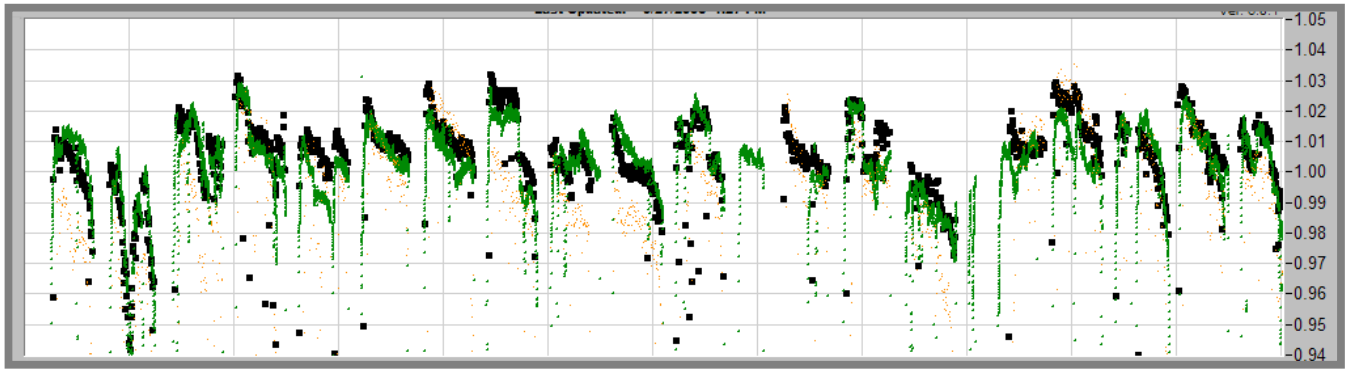

Fig. 2.8. Data Diagnostic Display showing the **Online Bottom Cell V_{OC}** and Offline Spire complete device (triple-junction) V_{OC} (■) and P_{MAX} (■) measurements for 16 consecutive runs. [Vertical: 1%/div; Horizontal: 50,000 meters full scale].

This figure plainly shows that:

- The Bottom Cell accounts for nearly all of the complete device V_{OC} variations observed in offline QA/QC, including the ≈ 2.5% (± 1%) drop in complete device V_{OC} from the beginning to the end of a coil. This 2.5% V_{OC} drop corresponds to a very significant 10% (± 4%) drop in the Bottom Cell V_{OC}.
- The drop in V_{OC} is also associated with an ≈ 2 - 4% drop in P_{MAX}.

Other online data not shown in Fig. 2.8 (the Bottom Cell Charging Rate for a far infrared light source) allow us to conclude that the V_{OC} drop is not caused by an increase in the percentage of germane in the bottom cell during a run. Figure 2.9 shows a screen capture of the online Data Diagnostics Display for two consecutive a-Si runs where the effect of the Backreflector can be clearly seen.

- *Upper Plot*: Offline Spire V_{OC} (■) and P_{MAX} (■) and online PVCD Bottom Cell V_{OC} (■) [1%/div]. The online Bottom Cell V_{OC} data (■) are taken with more than an order of magnitude finer spatial resolution than offline data; the offline data are usually delayed by several runs as shown in Fig. 2.8.
- *Middle Plot*: Two online Component Cell PVCD measurements of the Bottom Cell Charging Rate, strongly related to the cell short circuit current density, J_{SC} [5%/div]. These data are from the Bottom Component Cell PVCD. The data plotted in **purple** is the result of measurements made with an infrared LED light to clearly show the effect of changes in bandgap (e.g. germane concentration) effects. The **purple** vertical line marks a germane bottle change which resulted in a higher percentage of germane being incorporated in the cell, which consequently decreased the Bottom Cell bandgap which resulted in an increased infrared charging rate and decreased V_{OC}.
- Bottom Plot: Two measurements of the backreflector specular reflection taken from the spectrometers in the Payoff chamber of the a-Si machine. Reductions in specular reflectance can be a consequence of (combinations of) increased texture and increased scattered reflection, increased ZnO absorption, or decreased aluminum reflection.

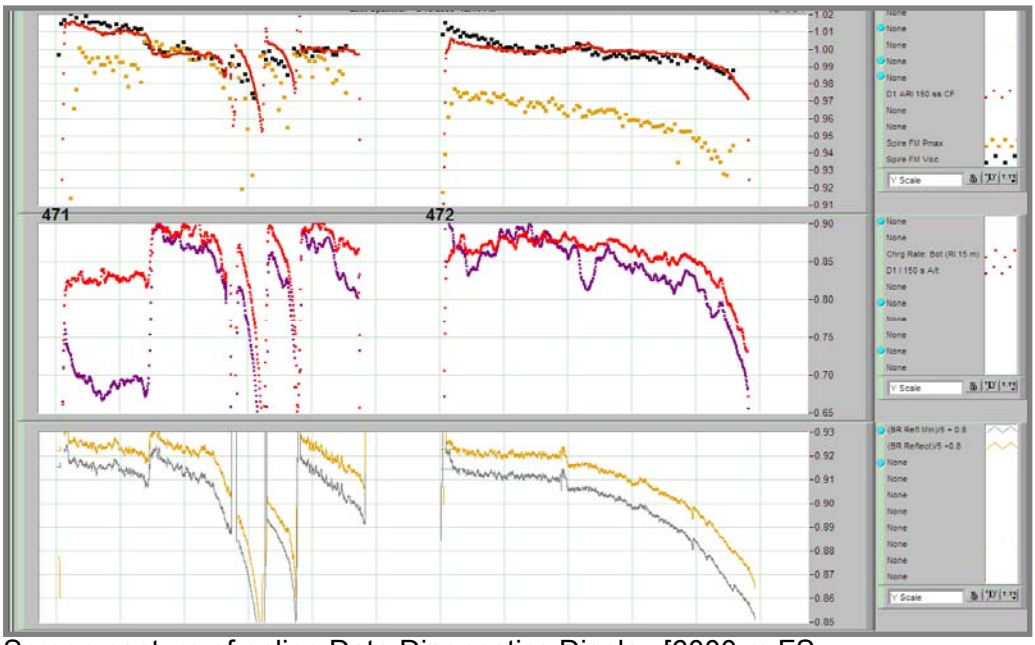

Fig. 2.9. Screen capture of online Data Diagnostics Display [6000 m FS

- The decrease in ***P*$_{MAX}$** [top plot] is highly correlated with decreased BR specular reflection [signal in bottom plot].
- The fact that the **Bottom Cell IR Charging Rate** signal in the middle plot decreases along with the **Bottom Cell *V*$_{OC}$** [top plot] tells us that this is not related to a changing germanium/silicon ratio in the intrinsic region.

These system variations have been mapped to specific process changes in the BR machine.

2.2.2 Near-term future uses of the PVCD System for QA/QC
Near Term Future Uses

The performance of these experimental devices has exceeded our expectations. While we have already demonstrated many of their uses for online QA/QC, they are perhaps rather under utilized as merely an online Acceptable/Non Acceptable indicator. Other uses for the PVCD system we envision in near future include:

- *Germane content stabilization*. In Section 2.2.1.d we illustrated the high degree of germane concentration control that could be provided by the Bottom Cell PVCD system.
- *Online cell matching and optimization*. The PVCD system can expedite the commissioning of future machines by optimizing the cell matching and germane content optimization online in few hours.

Figure 2.10 shows the measured changes in online measurement of the device charging rates and thickness in a series of experiments in which the web speed, and cell thicknesses, were varied by 5%.

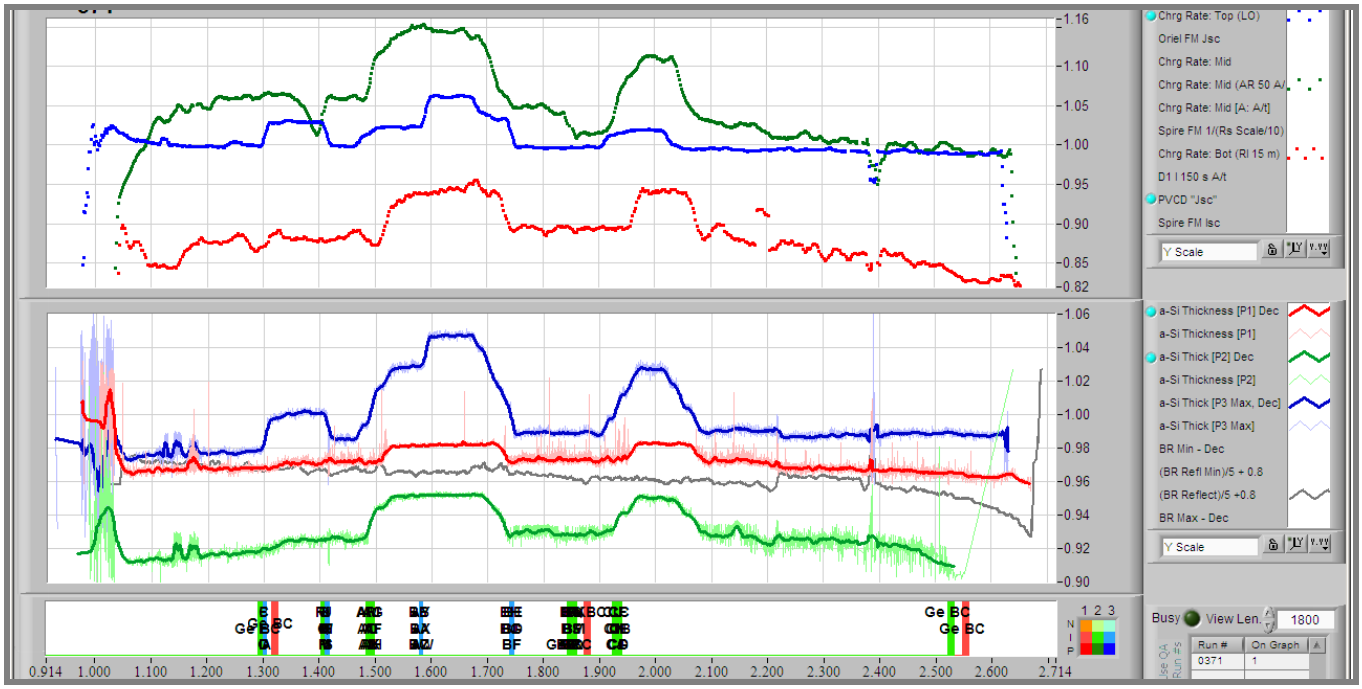

Fig. 2.10.. Online data from a run where there were 5% cell thickness and web speed changes. The online diagnostic systems have the precision to accurately see, and correct for, online, less than 1% changes [1800 m full scale].

Top Plot: Online PV Cell Charging Rate for the **Bottom**, **Middle**, and **Top** cells measured by the three component cell PVCD's in the AH-1 30 MW a-Si machine [5%/div].

Bottom: Online spectrometer thickness measurements for the **Bottom**, **Bottom + Middle**, and **Bottom + Middle + Top** cells [2%/div].

One can clearly see that the PVCD devices can easily resolve 1% changes in the thickness of each cell, and, the PVCD devices can maintain their charging rate calibration to the percent level for years. Consequently, we can envision sending a web from an existing production

machine through a new machine being commissioned to calibrate the PVCD devices, and then, online in a few hours, adjusting the new machine to precisely fabricate the same product as the existing machine. Today this process involves multiple runs, with intervening ITO deposition and offline QA/QC.

This same capability could also allow us to, online in a matter of hours, change the web speed and

- Adjust all the cells back to within 1% of their nominal thicknesses;
- Verify and adjust the bottom and middle cell bandgaps (Si/Ge ratio); and
- Verify that the doping layers are thick enough and of good quality.

2.2.3 Longer Term PVCD Uses

As great as the past and near term advantages of the PVCD system are, we see the greatest payoff in the future when we shall be operating a large number of production machines. The PVCD system hardware may have already demonstrated the potential to be initially calibrated, used to expedite commissioning, and then quite literally, operate for the lifetime of the machine with no need for service of electronics or re-calibration. Such a high degree of stability will become essential as the number of production machines grows exponentially. Even more important as the number of machines grows exponentially, is a system that will provide automated online QA/QC, optimization, and detection and pinpoint diagnosis of production problems. These systems, with their exceptional signal-to-noise ratio, high degree of stability, and high spatial resolution, will have primary importance in such an Expert System.

United Solar is in a phase of rapid expansion. Plans to expand production capacity to 300 MW (equivalent to 10 production machines) by 2010 have been announced. Continued growth at the industry average of about 40%/year would have us with the equivalent of about 100 machines by 2016. One could easily imagine the nightmare, or manpower requirements, to support many hundreds of systems that need monthly or annual light source changes and recalibration.

We believe that a fundamental requirement for diagnostic systems in such a vision is that they can be calibrated once prior to commissioning, and then operate for the lifetime of the machine without need of service or recalibration. We believe that we have perhaps already demonstrated this possibility. After 3 years of operation we have yet to see any measurable degradation of our solid state LED light sources. By reducing the repetition rate of the systems by order of magnitude, equivalent to the spatial resolution of the offline QA/QC measurements, we might expect these light sources to maintain this high degree of stability for 30 years, well beyond the expected lifetime of the production equipment.

As these diagnostic systems are continuously improved, and when these systems become supported by Expert Systems, we believe it is quite reasonable to expect a few individuals to be able to easily support automated optimization and precise pinpoint diagnosis of production problems in hundreds of production machines.

3. *DEPOSITION OPTIMIZATION AND PLASMA DIAGNOSTICS*

– Tim Ellison, Scot Jones, Tongyu Liu, Mark Lycette [ECD], **Gautam Ganguli** (United Solar)

3.1 Introduction and Summary

Work has concentrated on two principle area:

1. Investigation of the uses of plasma diagnostic systems to optimize the production process; and
2. Improvements and optimization of the deposition process.

3.2 Investigation of the Uses Of Plasma Diagnostic Systems to Optimize the Production Process

We have experimented with many technologies to diagnose the deposition process, including:

- Photo-detectors to monitor the light from plasmas;
- Gas conductivity monitors;
- Residual gas analyzers to analyze background contamination;
- Residual gas analyzers to monitor plasma reaction products;
- Spectrometers to monitor plasma reaction products

For all these systems, the following blanket statements are more or less true:

- Correlations can be found between plasma measurements and process conditions;
- Much less clear correlations can be found between plasma diagnostic system measurements and the PV device characteristics; and
- The correlations are usually valid for a specific working point; the calibration may vary significantly for different working points.

Or, quite simply, in a production environment, one good measurement of a property of the deposited device is worth a hundred measurements of the plasma properties. In order to provide feedback for the deposition process, where the device properties are controlled to the percent level, only a good direct measurement of the device property will suffice.

In this program we have developed a comprehensive system to measure the deposited device properties online, e.g.:

- The PVCD systems which allow precision measurement of the open circuit voltage, V_{OC}, and Charging Rate ($CR \alpha I_{SC}/C$) for each cell in the triple junction device, which also provides information on intra-cell series resistance;
- The cell thickness and the deposition profile for each deposition region in the a-Si machine;
- The thickness of the ZnO layer in the BR machine (under automated closed loop control), as well as the reflectivity and signals related to texture;
- The thickness (under automated closed-loop control), color, and signal related to conductivity of the ITO.

In the title of this research program is the word, “Comprehensive” – and so a good question to ask is, “In what way is our present diagnostic system not comprehensive”? And indeed, we he have two blind spots:

1. *Inter-cell series resistances (e.g. tunnel junction measurement)*.

   The PVCD system measures the device prior to application of ITO, charging each cell individually in a quintessentially open circuit condition; since there is no shunting from ITO, there is consequently no path to return current from the p3 layer to the n1 layer; absolutely no current flows between the p- and n-doped regions, or the tunnel junctions. Consequently we are almost blind to contamination in these areas [Fig. 3.1]

   Contamination in the very top of the p-layer, or the very bottom of the n-layer, such that the charging rate for the component cells is not affected but the tunnel junction is affected might seem, is at first glance, possible, though highly improbable. However, these regions are unique in that these are the only regions in the machine that we have installed water cooling, making the probability of a tunnel junction problem *a whole lot higher!*

   In this program we have addressed this blind spot in perhaps the most important way, by removing the water cooling:

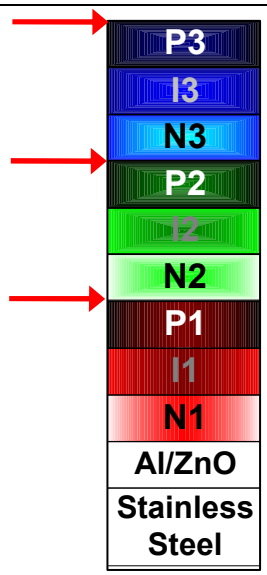

Fig.3.1. Present blind spots: contamination at between the p and n (including ITO) layer.

   - We designed and installed new “passive-cooling” systems to remove the water from the p-regions [Figs. 3.2–3]; and
   - We have also designed (and are now fabricating) a new “atrium design” Component Cell PVCD system [Figs. 2.2-3] which removes all the water and electrical feed-throughs from the system, and also provides better access.

   While we have consequently removed the proximate causes of inter-cell series resistances from the system, it may be years before our fears of such problems adjust to the new probabilities of leaks in these areas; and while the probability of contamination in these areas is now much reduced, to that of leaks in any other area of the machine, it is not zero.

2. *Desire for Complete Device Measurements*

   The Component Cell measurement provide us with a detailed view of the cell and allow easy diagnostics of the source of problems and variations; however, we ultimately need a complete device measurement or we are still, in some senses, operating in an open-loop mode (Table 3.I).

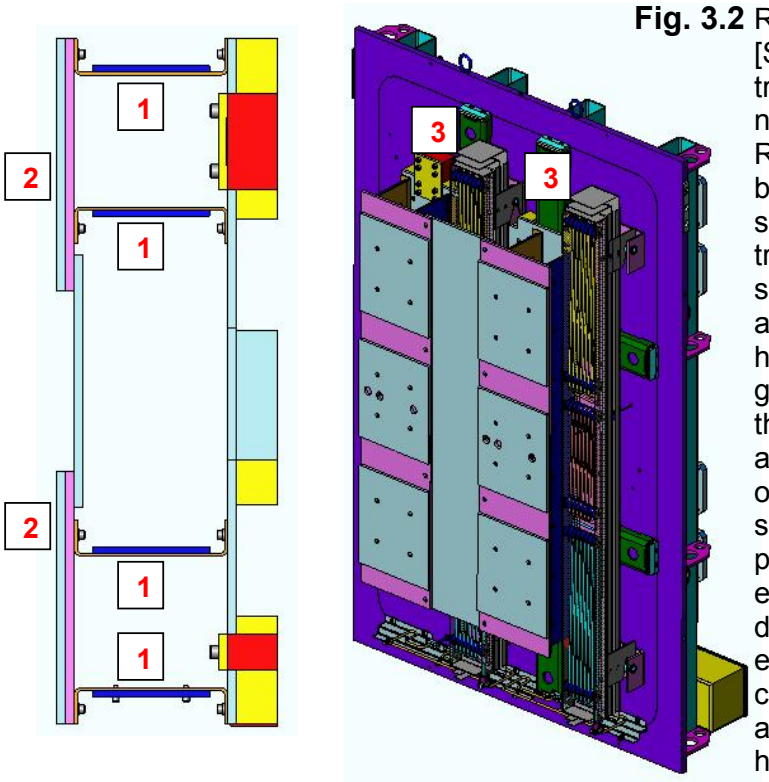

Fig. 3.2 Renderings of the new p-cooling system. [Side view, looking in the direction web transport direction, on the LHS, and view normal to the substrate surface on the RHS]. The aluminum plates close to the backside of the web [2] provide uniform substrate temperature. Heat is transferred to the door via the thin plates; shims [1] on these plates are used to adjust the temperature. This system also has provision to function as an rf grounding system; rf conductivity and thermal conductivity can be separately adjusted since the rf current flows only on the surface of the conductors. Also shown is the pre-heater and optional plate heater[3] to pre-heat the web as it enters the chamber and to adjust the deposition temperature to a greater extent online. By installing over-sized conductor shims, the temperature can be adjusted upwards using the second heater.

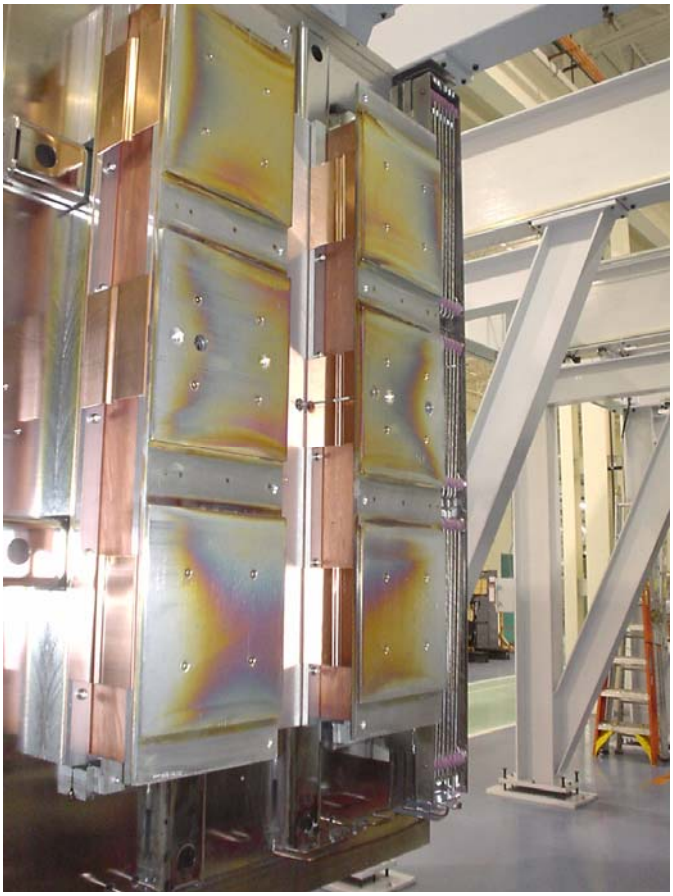

Fig. 3.3 New "Capacitive" p-cooling system installed for testing with a moving web in the 30 MW production equipment. The discoloration of the plates is from offline line testing in the "X" chamber at ECD's Plant 2.

Table 3.I. Principal advantages of online and offline diagnostic systems. The systems are complimentary.

Properties	Online Diagnostics	Offline QA/QC [Spire]	Online System Advantages/Disadvantages
Feedback Period	1 - 2 Hours	1-2 Weeks	X 100 feeback rate for QA, QC, and Optimization
Spatial Resolution	0.01 m - 2 m	25 m - 1000 m	X 10 Increased experimentation rate
Information	Details of Individual Layers, Component Cell, and Complete Device	Complete Device Only	Pinpoint problems and process variations
Product Certification	N/A	Good	Poor inter-cell effects characterization

An inline *I-V* measurement system, in combination with the present systems, provides us with all the advantages of both the inline and offline systems. We have consequently directed our efforts at designing and testing an *in-situ I-V* measurement system that will measure the complete device properties after application of ITO.

3.3. Inline I-V Measurement System

In this we summarize the development to date of this system which is now ready for installation and first testing in the 30 MW-I machine:

3.3.1. Study of times needed to measure the thin cells
  3.3.1.a. Pulsed mode; reduced intensity
  3.3.1.b. Single sweep measurement
3.3.2. Study of the effect of brushes contacting the ITO
3.3.3 Study of the effect of the ITO sheet and shunt resistances on the non-etched non-passivated material
3.3.4 Light source requirements, development, and testing
3.3.5 Electronics
3.3.6 Software

3.3.1. Investigations of the Spire Measurement System and Time Needed to Make Accurate *I-V* Measurements – in pulse mode, single-sweep mode, and at reduced intensities.

3.3.1.a Pulsed Measurements; Investigations using the Spire System

We have used the Spire *I-V* system to measure cell at reduced light levels in order to predict the performance of our product as a function of defect density as discussed in Section 4 [Yield Improvements]. We have had, however, some question about the validity of these measurements. We were curious about a couple (at least) things having to do with pulsed *I-V* measurements, e.g.:

- How long does it take for our thin, relatively high (> 100 times, with respect to crystalline) capacitance cells take to charge up and reach equilibrium?
- What about at reduced light intensities, where the charging time might be even an order of magnitude longer still?

So, we made some measurements. In looking at these data we found that:

- The 1 ms-long Spire pulse is not long enough to accurately measure the cell voltage for high load current *in the manner in which it is being measured*.
- The inaccuracy increases and can clearly be seen when the light level is reduced with neutral density filters.
- The trigger used in the present system is somewhat erratic – the light pulses and waveforms will jump back and forth on the scope when synched to the Spire data acquisition trigger.

Observations

AM 1.5 Measurements

Figure 3.4 shows waveforms from the Spire *I-V* measurement system. See caption for explanation of signals.

When the Spire flashes, we see the cell charge up to close to V_{OC} in the first 100 μs, before the light level reaches half its maximum value [**red box**]. At that point the current source pulses on [**violet box**]; the value to which the current initially goes is unknown – the op amp monitoring this signal saturates which gives the signals the flat cut-off level [**dark red dotted line**]. This pulls the cell voltage negative to about – 4 V. The current source then stabilizes at a constant value, and the cell begins to charge back up. When close to V_{OC}, the cell does reach a stable value; however, for higher load currents, where there is less current for charging the cell, the voltage never stabilizes; it is still rising when the voltage is sampled (t = 0), peaks after the measurement, and then falls as the light level decreases.

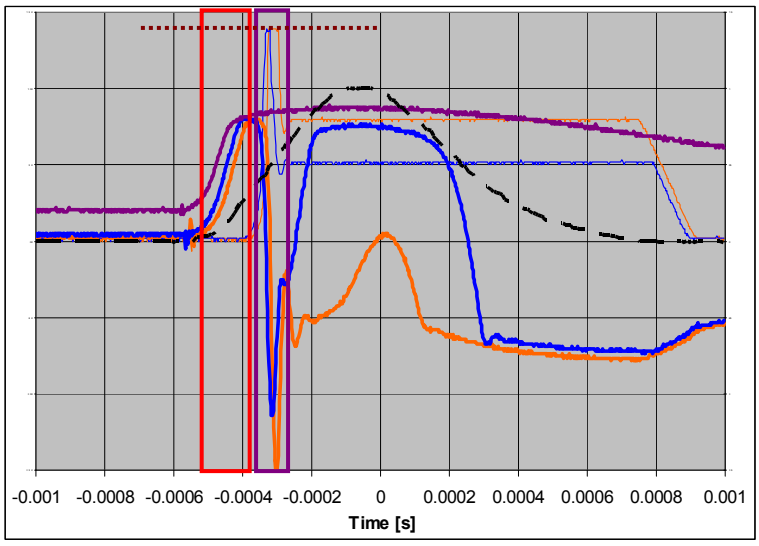

Fig. 3.4 Waveforms from Spire: dashed line: light pulse; thin lines are current and thick lines are voltage waveforms for measurements **close to short-circuit current** and **close to open circuit** (also **voltage waveform for open circuit**).

- Voltage measurements are <u>*under*</u>-estimated as the cell load current is increased;
- Voltage measurements might also be slightly <u>*over*</u>-estimated at V_{OC} (load current = 0): one can see that for no load the cell voltage drops slowly compared to the light level; the Spire peak-detector circuit will remember the V_{OC} measured at the higher light level prior to the measurement time. Of course this is a small (0.5 – 1% logarithmic) effect.

Measurements at Reduced Light Levels –

Since we are already seeing problems at AM 1.5, it's not surprising that the problems are exacerbated at lower light levels. For lower than AM 1.5 levels of insolation, as Figs. 3.5 show, not only does the voltage often not reach a stable value by the point of measurement, but the peak is shifted to a point well after the time-of-measurement when the light level is falling.

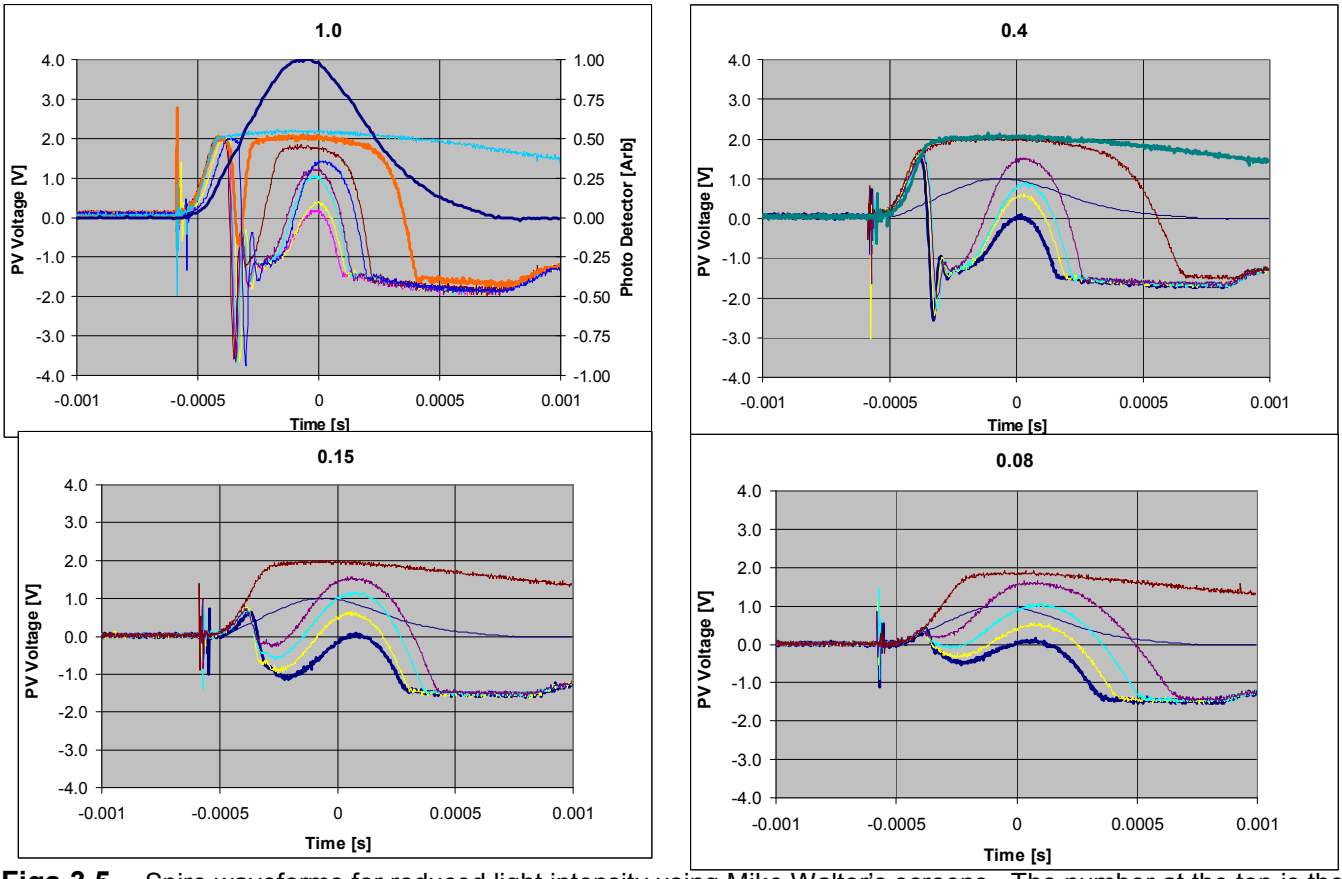

Figs 3.5. Spire waveforms for reduced light intensity using Mike Walter's screens. The number at the top is the relative light level.

These effects not only distort the *I-V* curve at low voltage/high current conditions, but also at the maximum power point. Figure 3.6 compares V_{OC} and P_{MAX} measurements made with a steady-state light source with pulsed-Spire measurements.

In the steady-state (Baojie) study, the P_{MAX} and V_{OC} both fall-off closely following a logarithmic curve; the Spire-measured P_{MAX} measurements, however, show a much more rapid fall-off at reduced levels of insolation.

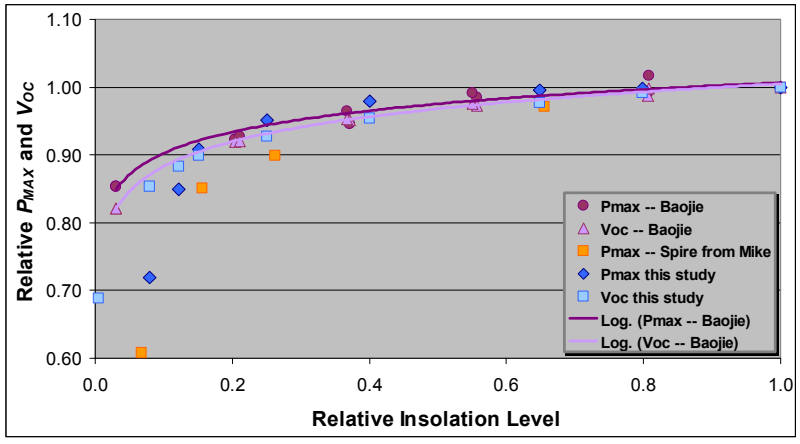

Fig. 3.6. P_{MAX} and V_{OC} measurements made with a steady state source and with the Pulsed-Spire. Relative P_{MAX} is P_{MAX}/J_{SC}; relative V_{OC} is $V_{OC}/V_{OC,\ AM\ 1.5}$.

Just How Long of a Pulse Do We Need?

We see cell voltage rise-times of as little as 70 μs for cells with no load and the Spire light source reaching only 50% of its maximum value and so expect we could see rise times of about 35 μs at AM 1.5 levels *for no load*. BUT – these measurements did not have the resolution to show whether we see longer-time-constant effects at the percent level.

3.3.1.b Cell Measurement Times for Single-Sweep Measurements

We continued our investigations of the length of time needed to obtain accurate *I-V* measurements for our thin-film high-capacitance solar cells. This is of interest to us for a couple of reasons:

- We have documented that the pulsed Spire simulator reads low when measuring at reduced light intensities; and
- we want to investigate the possibility of making a full *I-V* scan in a single light pulse.

We build a current-controlled *I-V* sweep system and tested cells under the Oriel DC light source. As shown in Figs. 3.7-8, we begin to see significant distortion of the measured I-V curve for sweep times of less than about 3 ms. In these figures, the legend refers to the total sweep time; the time to sweep over the range of interest, however, is about 60% of this time.

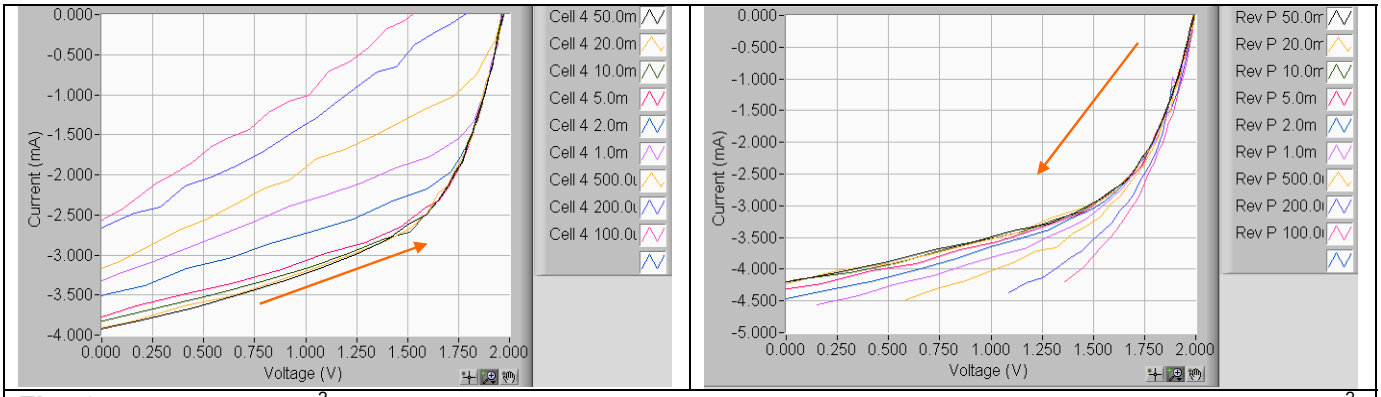

Fig. 3.7 QA cell [10 cm^2] *I-V* measurements taken at a range of sweep-rates with an insolation of 560 W/m^2. Left: sweep from J_{SC} to V_{OC}; Right: sweep from V_{OC} to J_{SC}. [The displayed current is $1/10^{th}$ the actual current].

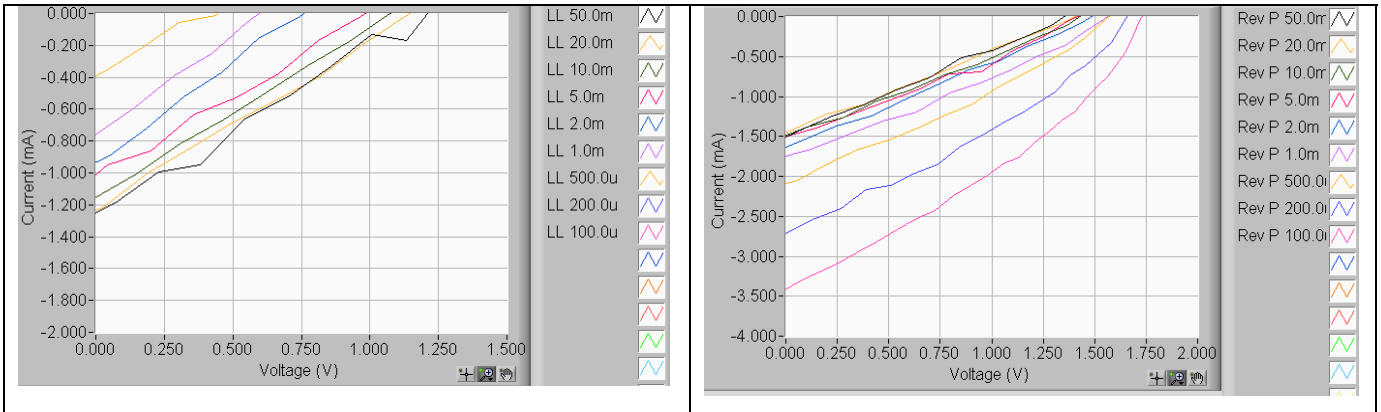

Fig. 3.8 QA cell [10 cm^2] *I-V* measurements taken at a range of sweep-rates with an intensity of 100 W/m^2. Left: sweep from J_{SC} to V_{OC}; Right: sweep from V_{OC} to J_{SC}. [The displayed current is $1/10^{th}$ the actual current].

We also looked at the time response of the solar cell. In Table 3.II and Fig. 3.9 we show the time needed for the cell voltage to settle to various levels after a step change is made in the solar cell current.

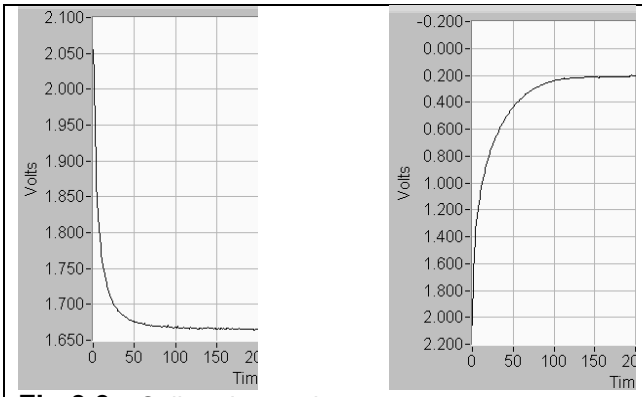

Fig.3.9. Cell voltage time-response as the cell current is stepped from 0 to I_{MP} [left], and from 0 to close to I_{SC} [right]. [100 μs/div (2 μs/data point)].

Table 3.II. Summary of solar cell settling times vs. measurement accuracy for the two current steps shown in Fig. 10.

Table II. Cell response times.

Measurement accuracy	Settling Time [μs] V_{OC} to V_{MP}	V_{OC} to J_{SC}
10%	20	100
5%	40	150
2%	50	200
1.00%	80	300
0.50%	150	
0.20%	200	

Some of the tentative conclusions we have thus far include:

- The cell equilibration times could be reduced by designing the *V-I* measurement circuit to specify the cell voltage, and have a current capability in excess of that of the solar cell – especially for discharging the cell.
- There isn't "one number": the time depends upon the measurement being made, and how the measurement is performed.
- A 5% accurate measurement might be very accurate if calibrated against a higher accuracy measurement and performed in the same way – for a product with fairly constant cell properties.

3.3.2. Cell Measurement Techniques – Effect of Brushes on the Material

We investigated of the use of brushes to make contacting *I-V* measurements inline in the ITO machine. Such a system, in combination with inline-ITO deposition, would reduce the delay in getting *I-V* measurements by about a factor of 200.

We have used brushes in the past for measurements of the shunt resistance and ITO sheet resistance – measurements which draw very little current, e.g. < 100 μA. Cell *I-V* measurements would require drawing a few more orders of magnitude of current through the brushes – something which we worried might damage the web. We consequently decided to perform experiments to determine how much current could be drawn though a brush before causing damage.

The experiments were performed as follows:

- On a series of cells, prior to passivation and etching, currents in the range of 1 μA to 100 mA were drawn through a single brush on the cell. The brush was moved across the cell at the same speed that the web moves in the ITO deposition machine.
- The experiments were performed both with cells illuminated by a solar simulator, and with cells at very low light levels (in which case we reversed the polarity of the current to keep the PV diodes forward biased).
- All the cells, along with two sets of controls (cells that were never touched by a brush, and cells touched by a brush but with no current) were then sent through the cell line. We looked for damage by:

- Visual inspection (e.g. passivation marks or discoloration);
- Measurement of the cell shunt resistance; and
- Measurement of the cell P_{MAX} at AM 1.5.

We saw no visual evidence of cell damage. Electrical measurements, as shown in Fig. 3.10, also showed no correlation with brush current.

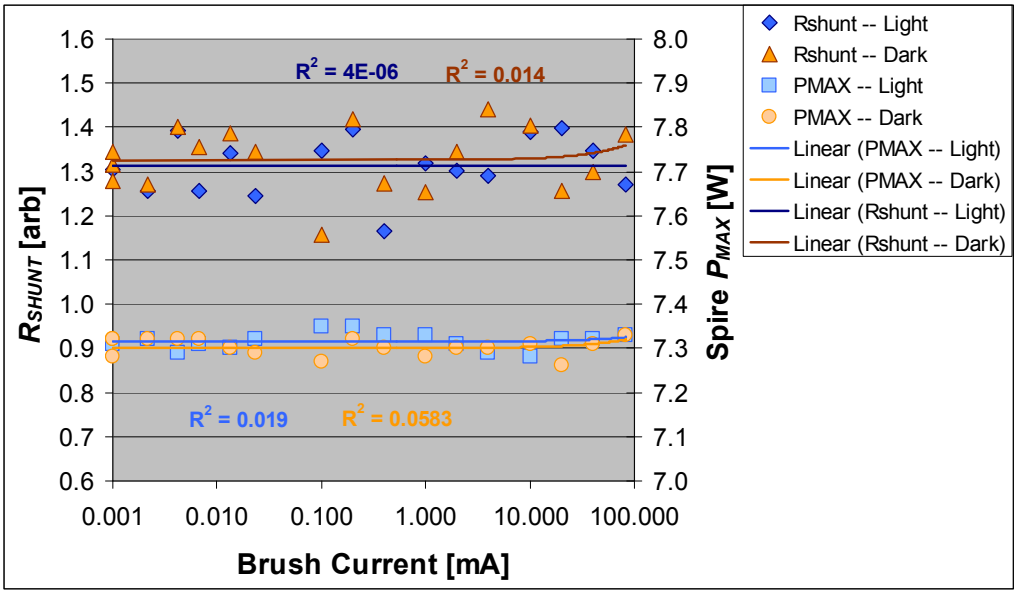

Fig. 3.10 Cell shunt resistance and Spire P_{MAX} as a function of brush current. The was no visual cell damage or variation in cell electrical properties correlated with the brush current.

This was an exciting result: it shows that we can easily draw short circuit currents at AM 1.5 insolation levels from brushes without damaging the web – a necessary prerequisite for measuring *I-V* curves inline in the ITO machine.

3.3.3 Sheet and Shunt Resistance Measurements and Affects on *I-V* Measurement

Accurate online measurements of the ITO sheet resistance and device shunt resistance will be necessary to correct the *I-V* curves made *in-situ* after application of ITO but prior to the etching and passivation processes – processes that reduce the degree of shunts and eliminate shunts at the edges of the material.

The shunt and sheet resistances are coupled together:

- The shunt resistance is limited by the sheet resistance because of the high current densities at the point of shunting, as shown in Fig. 3.11.
- The sheet resistance also is affected by the shunt resistance since multiple shunts provide parallel paths for the sheet current. This effect becomes more apparent, as might be expected, as the distance over which the sheet resistance is measured is increased, as shown in Fig. 3.12.

Reliable online and de-coupled R_{SHEET} and R_{SHUNT} measurements will be necessary to correct the online *I-V* measurements. We are developing these measurement systems and will test them in the ITO deposition machine.

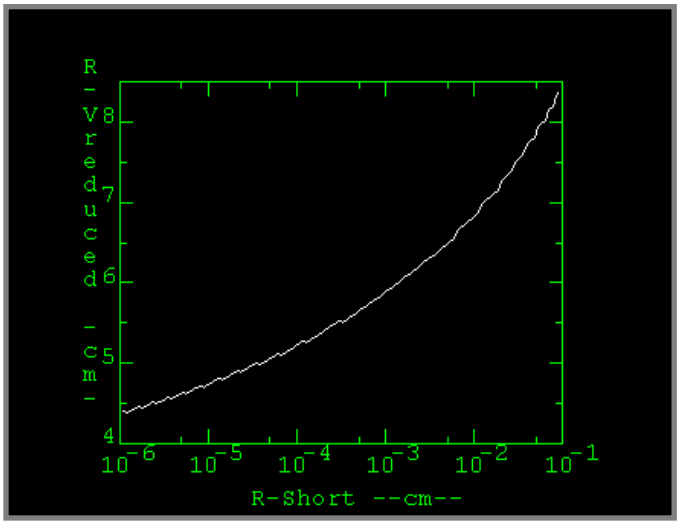

Fig. 3.11 Radius of reduced voltage as a function of the radius of the shorted area for low current densities (0.5% AM 1.5). As the radius of the shunted area is increased by a factor of 10^5, from the thickness of the film to 1 mm, the radius of the reduced voltage area increases by a factor of 2 from about 4 to 8 cm.

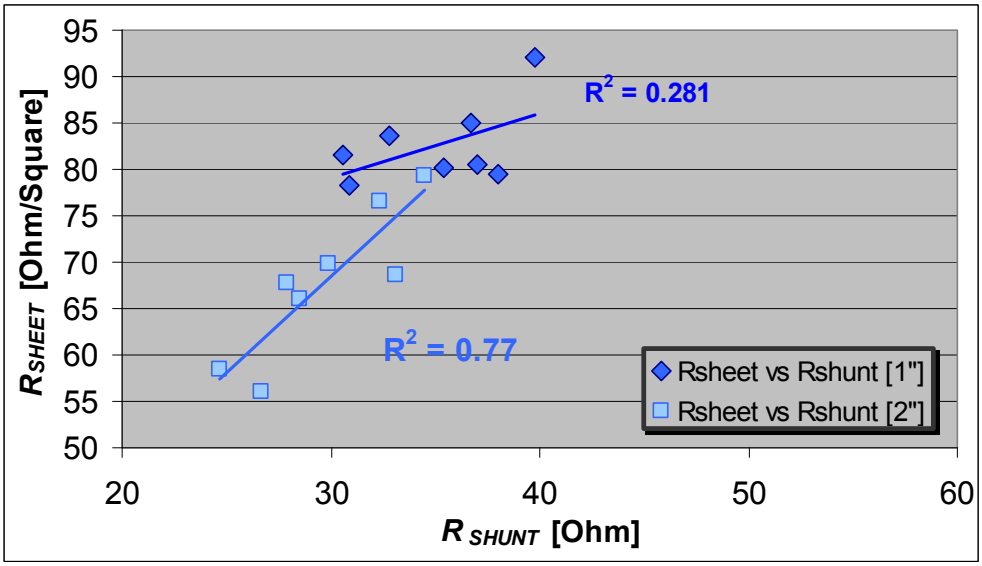

Fig. 3.12 Raw R_{SHEET} measurements as a function of raw R_{SHUNT} measurements for non-etched and non-passivated samples for two different measurement geometries.

Measurement of I-V Characteristics of non-etched non-passivated PV

We tested measurement of PV device *I-V* curves on PV material prior to etching and passivation to test the feasibility of full *I-V* measurements in the ITO machine. The I-V curves were trivial, as shown in Fig. 3.13 (left), in that the measurement described perfect resistors; the resistance being low enough that even at V_{OC}, all the light-generated current passed through the shunts and the diodes in the PV devices never began conducting.

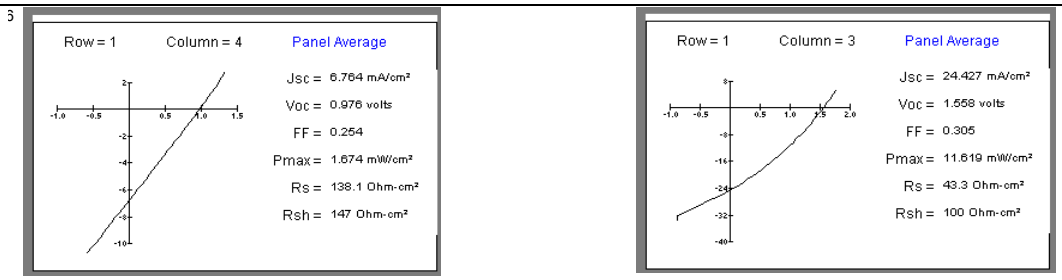

Fig. 3.13. I-V curves for a 1" (left) and 2" (right) diameter area of a 14" wide cell illuminated 60% of AM 1.5 intensity. The cell has not been etched or passivated.

The principle shorting mechanism is the combination of ITO sheet conductivity and shunting outside the measurement area, including the shorting at the edges of the non-etched cells. This is demonstrated by making the same measurement but on a larger area, as shown in Fig. 3.13 (right), since the ratio of the measurement area to the perimeter shunt increases in proportion to the diameter of the measurement area.

We conjecture that the effect of the shunts surrounding the area being measured can be eliminated by using two sets of contact brushes as shown in Fig. 3.14: the inner set to measure the *I-V* curve of the illuminated area, and an outer set, powered by a separate power supply, to provide the necessary current to the shunts surrounding the measurement area.

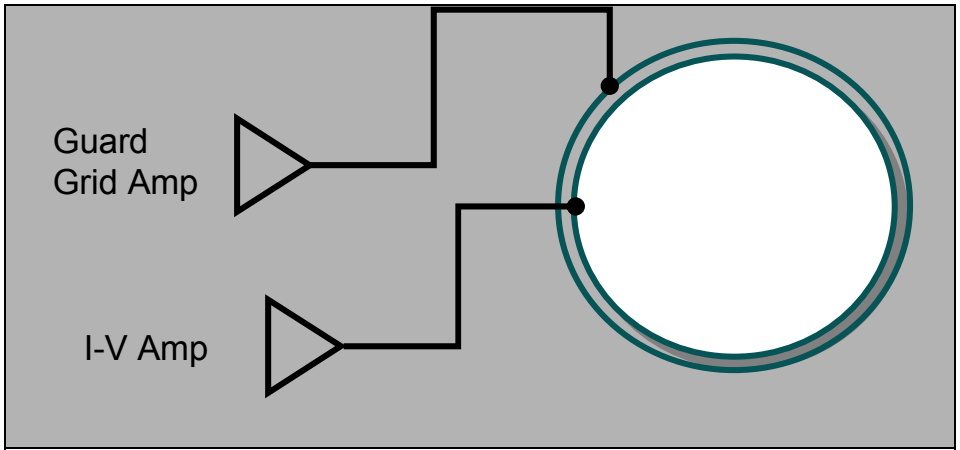

Fig. 3.14. Schematic of proposed technique to eliminate the effect of shunts surrounding a small illuminated measurement area on a cell prior to etching and passivation.

We procured power supplies, wrote software, and built hardware to test this concept. The results, shown in Fig. 3.15, are promising;

- A dark measurement provides an accurate measurement of the resistive shunt resistance, and this value can be used to remove the effect of these shunts from the I-V curve. At high light intensities in a passivated cell, the effective shunt resistance is due only to recombination current, so removing this resistance is justified. As shown in Fig. 3.15, this fix moves the test *in-situ I-V* curve into agreement with an AM 1.5 measurement at the I_{SC} end of the curve (**blue curve**, Fig. 3.15).
- The "grids" in the test *in-situ I-V* are about twice the distance apart as in the completed cell measured in the Spire, increasing the series resistance. Adding a small series resistance correction (**orange curve**, Fig. 3.15) brings the slope of the test *in-situ I-V* curve into agreement with the offline Spire curve. The in-situ system will also perform ITO sheet resistance measurements to also allow real-time correction of the *I-V* curve.
- After both these corrections, we still see the test *in-situ I-V* curve V_{OC} below the AM 1.5 Spire measurement. Most of this shift is due to the logarithmic dependence of V_{OC} on light intensity and the lower light intensity and increased shadowing used in the test fixture.

On the basis of these results we moved ahead to finish engineering of the first generation system for testing in the 25 MW production equipment.

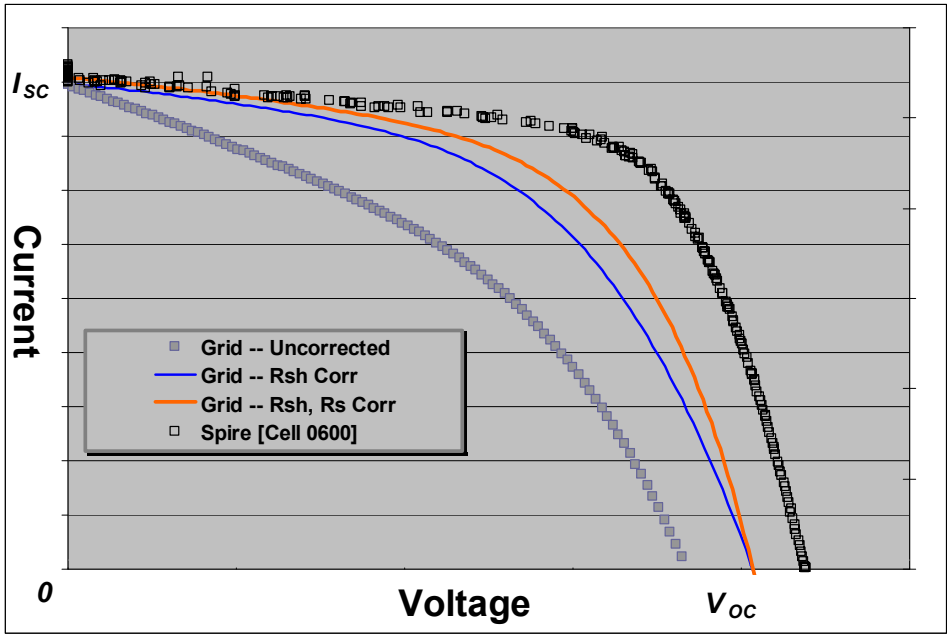

Fig. 3.15 Measurements from bench-test *in-situ I-V* measurements system using "guard electrode" and a Spire measurement of a completed cell. See text for explanation.

Unlike the PVCD's, the *I-V* system needs to make contact with the surface of the web to draw current from the device. A key to making this work is a set of contacts that can draw current from the web without damaging the web and minimizing the amount of shadowing. We worked with a brush manufacturer that makes conductive brushes for static applications to develop brushes for our application. We then designed a brush holder and mounting system for these brushes, as shown in Figs. 3.16-17.

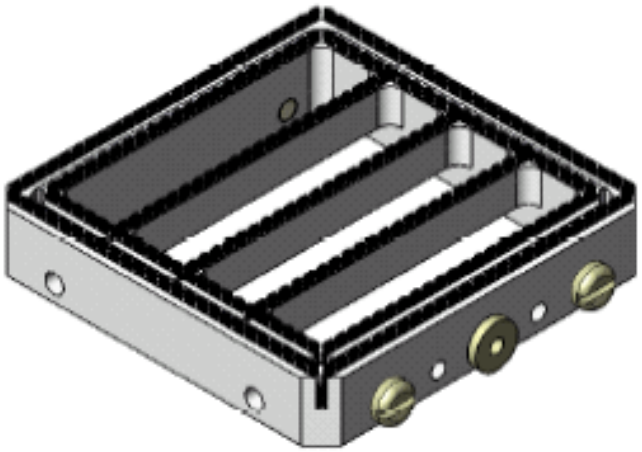

Fig. 3.16 ITO *I-V* system brush holder.

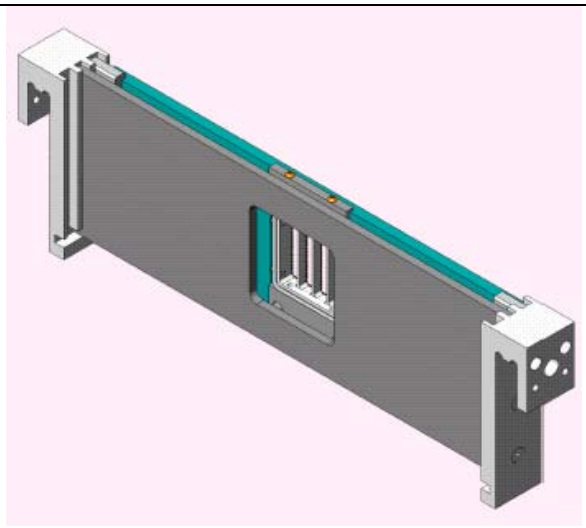

Fig. 3.17. Mounting system for brush holder.

We also tested these brushes for web-damaging effects. In our tests, as shown in Figs. 3.18-19, we observed no statistically-significant difference in the electrical properties of control cells, cells that made contact with the brushes, and cells that made contact with the brushes and had much higher current densities in the brushes than cells will have in normal operation.

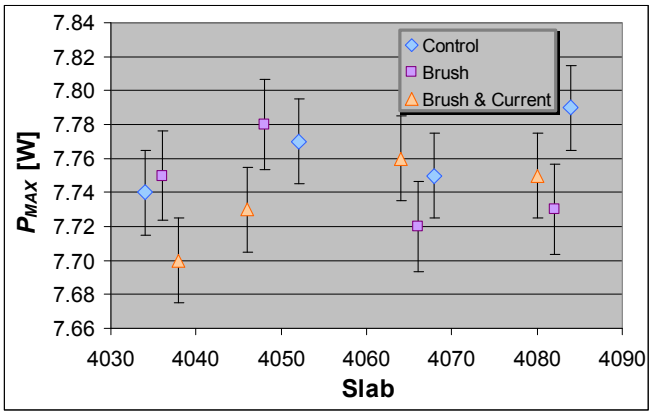

Fig. 3.18. Measured slab power.

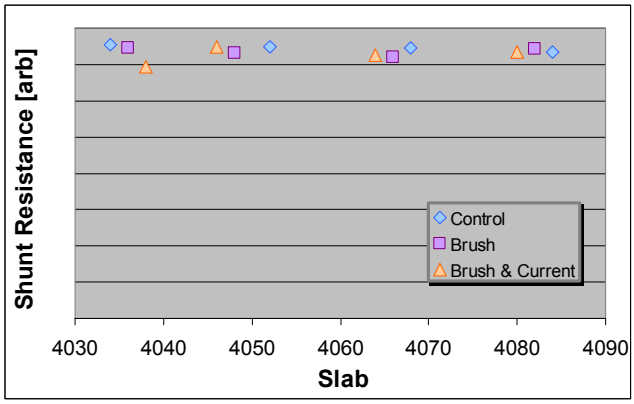

Fig. 3.19. Measured slab shunt resistance.

3.3.4. LED Light Source Development/Extreme Reliability

ECD has recently announced that United Solar Ovonic will have a manufacturing capacity of 300 MW by 2010 – equivalent to 10 production machines. Assuming USO continues to expand at the industry rate, the number will approximately double every 2 years. In this coming regime we shall literally have on the order of 100 online diagnostic systems with their number continuing to grow exponentially. We see the need, and the possibility as demonstrated by the performance of the PVCD systems, to design systems that do not require routine maintenance, service, or even calibration; literally, systems that will be installed to expedite the commissioning process and continue to operate, without need for service or calibration, for the lifetime of the manufacturing equipment, always providing the same reading for product with the same characteristics.

Figure 3.20 provides a glimpse of this degree of reliability. It is a record of the top cell charging rate, *CR*, measured over the last 3 years [about 400 runs, or 0.8 million meters of web] from the a-Si TU PVCD. This signal has maintained its integrity, accuracy, and precision over this period without calibration or service [other than twice annual dusting].

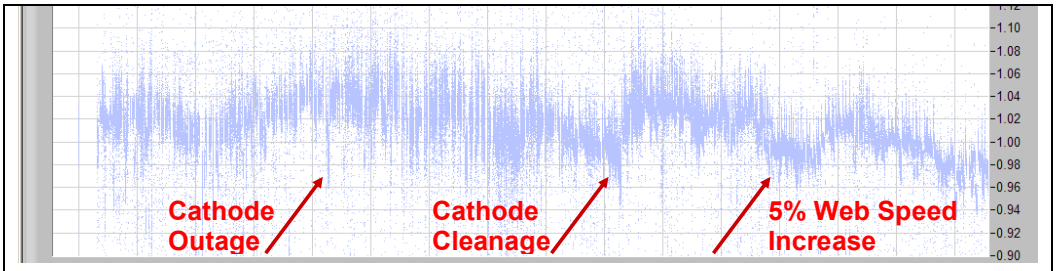

Fig. 3.20. Raw data for top-cell charging rate, *CR,* over last 400 runs [Vertical: 2%/div; Horizontal: 800 km FS]. A few operating events affecting the CR measurement are shown.

This high degree of reliability is made possible by the use of a solid state LED light source which, if operated within limits, could enable operation without need for maintenance or calibration for more than 10 years. Table 3.III shows a comparison of possible light sources available for use in the ITO *I-V* measurement system.

Table 3.III. Comparison of Light Source Possibilities for the online ITO *I-V* System.

	Pulsed	DC	LED
I-V Measurements			
Accuracy	**Suspect**	**Good**	**Good**
Ease	**Harder**	**Easy**	**Easy**
Lifetime	**Year?**	**1 month**	**10 - 100 yr [Est]**
Spectrum			
Measurement	**Difficult**	**Easy**	**Easy**
Time Dependence	**During Aging**	**Aging**	**Aging?**
	During Pulse		**Can be corrected**
Class A	**Y**	**Y**	**N, but can match I**
Availability			
Small Area	**N**	**Y**	**Y**
Long Pulse	**N**		**Y**
Horizontal Config	**??**	**Not Std, Class B?**	**Y**
Lead Time	**n/a**	**10 - 12 Weeks?**	**Couple Weeks**
Un-Reliability	**n/a**	**Doubtful**	**Highly Probable**

The LED light source developed by ECD would be our choice for such highly reliable systems. There is only one drawback: diodes with the wavelengths and intensities necessary to build a Class A solar simulator are not yet commercially available; the principle problem is the relative low intensity of the diodes in the amber/green band, as shown in Fig. 3.21. (For the highly reliable systems we envision, we are, for now, not considering the use of phosphor-LED's, since the phosphors can age with use/time).

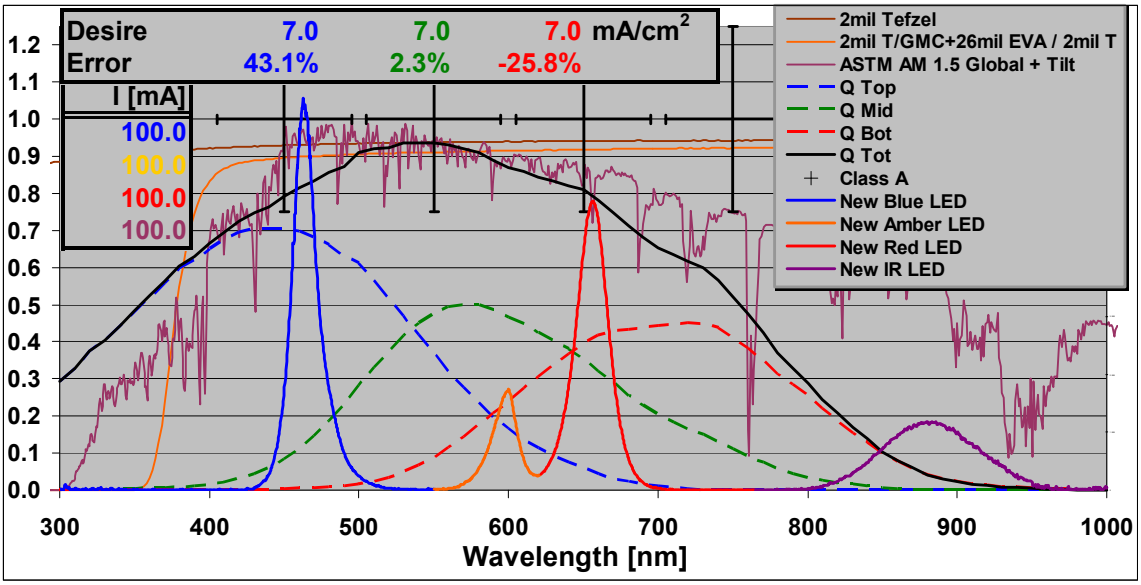

Fig. 3.21 The AM 1.5 spectrum, lamination transmission, quantum efficiency of the triple junction product, Class A wavelength and power density requirements, and spectral radiometer measurements of the ECD PVCD **Blue**, **Amber**, **Red** and **Infrared** LED solid state light source for 100 mA current in each diode string.

We can, however, ask a different question: rather than asking whether we can build a Class A simulator, which allows a ± 25% power density error in each of the six wavelength bins, we could ask the following question: can we build a solid state light source that matches the current in each of the component cells of our triple junction device at AM 1.5 levels? The answer to that question appears to be YES. As summarized in Table 3.IV:

- Using just two LED colors (Blue and Red) we can match the current within all three cells to within **2.5%** [Scenario 2].
- Using 3 LED colors (Blue, Amber and Red), there is a unique set of LED currents that will exactly match the current within all three cells [Scenario 3]; and as shown in Scenarios 4 – 5,
- Using 4 LED colors (Blue, Amber, Red, and **Infrared**) there exist an infinite number of solutions to match the current in all three cells [e.g. scenarios 4 – 5].
-

Table 3.IV. Scenarios for balancing currents at the AM 1.5 light level in the triple junction device using our existing LED Light Source.

Scenario	Current in LED String [mA]				Current Error In Cells [Target: 7 mA/cm^2]		
	Blue	Amber	Red	Infrared	Top	Middle	Bottom
1	100	100	100	100	43%	2%	-26%
2	55	0	161	0	1%	-2%	2%
3	54	38	152	0	0%	0%	0%
4	53	80	137	100	0%	0%	0%
5	50	200	93	382	0%	0%	0%

Optical Measurements of the intensity vs. position for each of the 4 colored LED's in the LED array were completed. A small subset of these data are shown in Fig. 3.22. The data provide a 3-D map: intensity as a function of x-y position, on a 0.5 inch grid, as a function of distance (z position) from the detector for each of the LED diode families. These measurements will help us dead-reckon the relative intensities of the different LED colors to provide the same current-matching in the triple junction device as does the AM 1.5 spectrum.

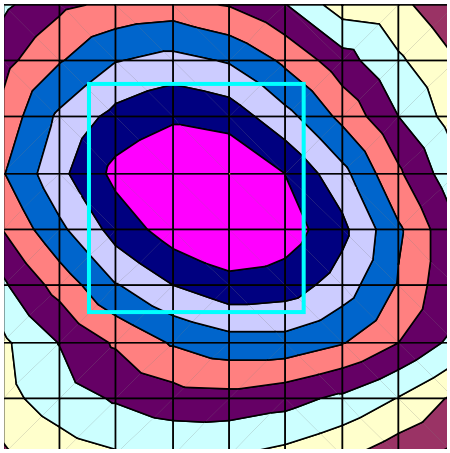

Fig. 3.22. Plot showing intensity vs. position for Blue LED's at a fixed distance from the array. The Blue Box shows the area of our first prototype *I-V* brush system.

3.3.5. Electronics Chassis

The ECD Machine Division Electronics Department professionally packaged of the PVCD electronics for the 25 MW II facility, as shown in Fig. 3.2.23. Due to historical data-acquisition limitations, in the past we were limited to operating all LED colors with the same current. The first of these new chassis off the assembly line was modified to be used for the testing of the post-ITO-deposition *in-situ V-I* measurement system under development. The electronics were modified to allow independent control of each color of LED; this will allow us to adjust the spectrum to cause the same current in each cell of the triple junction device as there would be when the device is illuminated by the AM 1.5 spectrum.

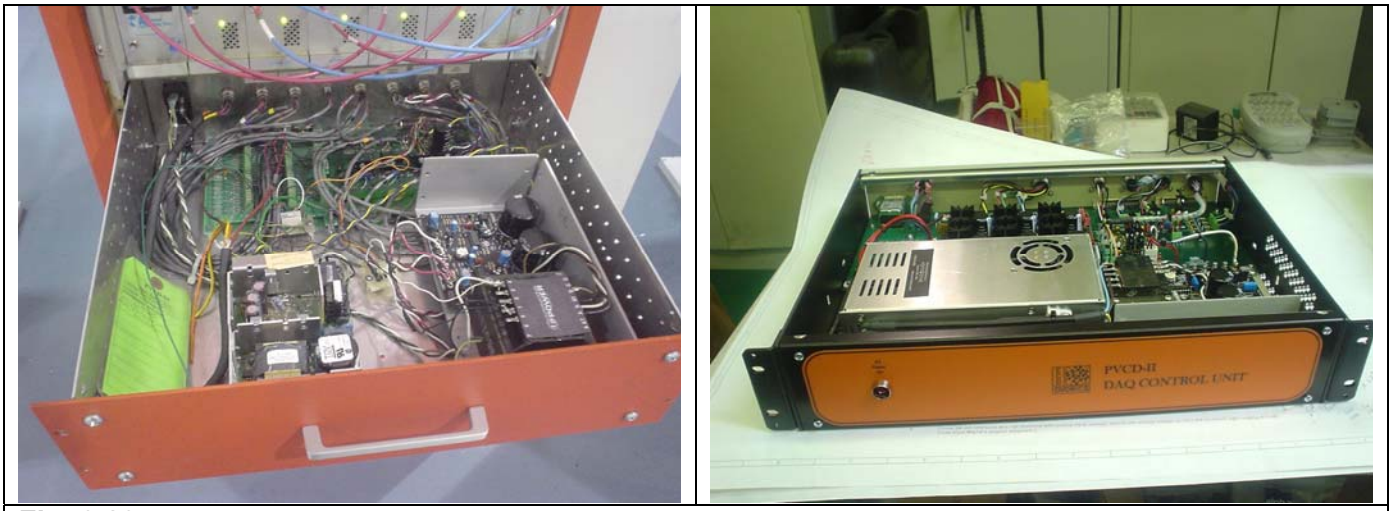

Fig. 3.23. PVCD electronics chassis – Left: development chassis used in the first 25 MW production plant; Right: new professionally-packaged PVCD electronics chassis developed for the 2nd 25 MW facility.

This feature will also allow us to:

- Set the light levels for the different wavelengths so as to provide the same current in each cell as would an AM 1.5 spectrum. There are an infinite number of combinations of the 4 LED wavelengths that can be used; we plan to use of two or three of these combinations for a consistency check.

- Online, measure efficiency as a function of insolation level;
- The light source can be instantly varied from AM 1.5 to AM 0, or to simulate the effects of absorption in the later-applied lamination material; and
- The light source spectrum can be varied to simulate, online, the effect of increasing or decreasing the thickness of each intrinsic layer in the triple junction device.

3.3.6. Software

We completed initial specifications and have written and tested software for the *I-V* measurement system software. We see 3 possibilities:

1. Single Point: "Spire-Like" system: single data-point/light pulse
2. Full Curve: full *I-V* curve in single longer light pulse
3. Hybrid (e.g., a few long pulses to get full *I-V* curve, with "smart" ramp

The Single Point (1st) Possibility will definitely work and is straightforward. The Full Curve (2nd) Possibility is much more preferable:

- More data (e.g., cell-by-cell characterization);
- Much (1 - 2 order of magnitude) longer LED lifetime.

The Full Curve (2nd) Possibility will take much more development – many things will be close to their limits (e.g., solar cell time constant, LED pulse lengths, power supply and monitoring electronics bandwidths); furthermore, the LED output will vary within pulse since we do not yet have light feedback.

We shall begin with Possibility #1. We shall use this straightforward technique to "get on the air", and then in parallel develop Possibility #2. We shall be able to use the results of Possibility #1 to test/check the accuracy of Possibility #2.

4. YIELD IMPROVEMENTS

Jon Call, Mike Walters [USO]; Tim Ellison, Rob Kopf [ECD]

4.1 SUMMARY

In this work we:

- Identified the largest source of yield loss in production: defects.
- Chose an online measurement criterion to quantify degree of defects.
- Correlated defect level measurement to:
  - Initial and stabilized cell and module performance;
  - Cell performance after accelerated testing; and
  - Cell and module performance as a function of insolation level using both solar simulator and long term outdoor testing.
- Recommend a new cell-line criterion to USO management; the criterion was accepted.
- Carried out a long-term outdoor exposure test to look at the effect of defect density in cells over time.

The results of this work, carried out by the USO QA/QC department and ECD was a new cell line measurement criterion for defect density and a significant (5 – 10%) increase yield and (10 – 15%) increase in throughput. While most of this work was completed in the Spring and Summer of 2005, outdoor testing has been, and is, continuing. We are also continuing our investigations of the effect of defects on cell performance for low light conditions, and the accuracy of our measurements at low light conditions using a pulsed simulator.

4.2. BACKGROUND

Most, but not all, defects are removed in our proprietary passivation process; however, a few defects may remain. In the cell line we quantify the degree of defects and sort the cells accordingly. As shown in Fig. 4.1, at STC we observe no effect on the module P_{MAX} as a function of defect density, even for the highest degrees of defects encountered in production.

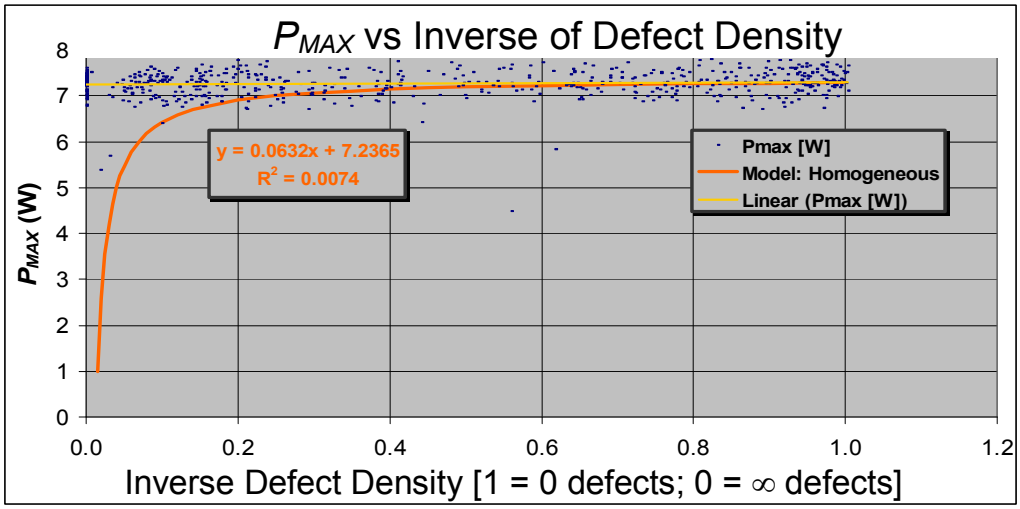

Fig. 4.1. Measured P_{MAX} as a function of Defect Density. The gold line is a linear fit to measured data; the dark orange line is a model that creates a similar shunt resistance uniformly across the cell. Discreet defects behave fundamentally different.

As also observed in Fig. 1, few discreet defects affect the cell differently than continuous homogenous defects. We believe that is due to the fact that the influence area of a shunt decreases as a function of light intensity on the cell. As shown in Fig. 4.2, the calculated influence area for a defect creating a dead short between the ITO and Backreflector is relatively independent of the size of the defect, and decreases approximately proportionally to the light intensity as a consequence of the ITO resistance.

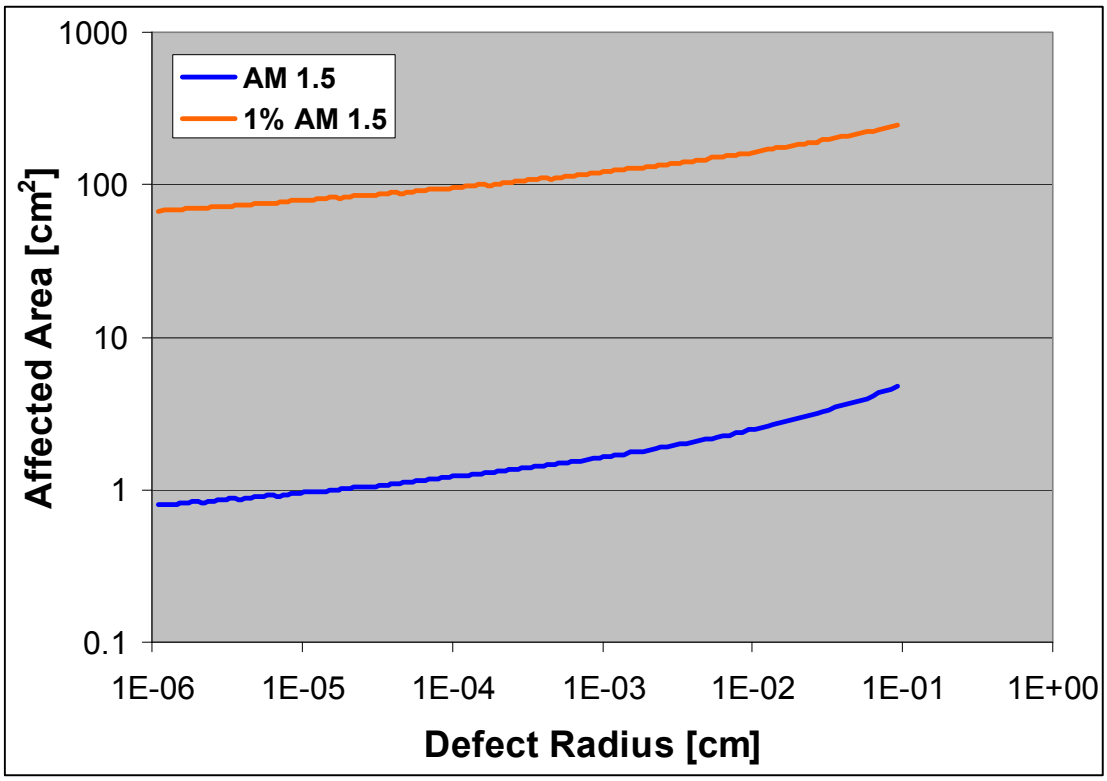

Fig. 4.2. Numerically calculated affected area as a function of defect radius.

Consequently, in principle, a few shunts should not be able to affect the power output of our 800+ cm^2 cell, though the effect might be seen at lower levels of insolation when affected area increases. We confirmed this result using the Spire simulator, and also investigated whether the degree of defect density affected the results of light soaking and accelerated tested. To further confirm our results, for perhaps even a single defect might somehow affect the cell quality over time, we also performed outdoor testing.

4.3 Cell Sorting:

We began work by collecting samples over a few months of operation and sorting them into 5 “bins” with varying degrees of defects. This extended collection period was necessary for two reasons:

1. We wanted to ensure that the samples in each bin were “typical”: although we have identified the primary source of defects, defect density levels variations might arise from many source and be affected by many operational variations. We did not want to select

for a particular type or source of defect, or fill bins with an atypical or peculiar type of defect.

2. We wanted to test material well outside of both the present and the projected acceptance levels of defect density in order to ensure that the criterion level was in a regime where the cell characteristics did not change rapidly with the defect measurement (i.e., we did not want to set the acceptance level close to a "cliff"). This range of bins would also allow us to make predictions about yield and performance as a function of criterion level. We consequently needed to look at a large number of samples to find enough "outliers" to fill the extreme bin ranges. Even after an extended period, we were unsuccessful in filling the extreme bin ranges and so performed a special production run to deliberately make a small amount of higher defect-density material for these tests.

In the course of creating these Bins, measuring the samples, and designing the experimental procedure, we changed the number of Bins to 3: this allowed us to have better statistics and reduce the number of samples needed to send through accelerated testing and outdoor testing. The number of bins was arbitrary and merely a tool for initial selection of samples: each bin was populated with a range of defect levels and the data can later be plotted continuously or a function of new arbitrary Bins.

The experimental procedure for this work is summarized in Fig. 4.3.

4.4 Summary of Results of Indoor Studies

We performed Thermal Cycling (TC) and Humidity Freeze (HF) measurements and 800 hour Light Soak (LS) tests of cells with a range of defect densities. Cells (124 L-slabs) were grouped into three Bins. We describe the tests and summarize the measurements showing a statistically-significant correlation with defect density level prior to, and after, accelerated testing. We found that:

- There were no "catastrophic" reductions in P_{MAX} at AM 1.5 that could be attributed to even the highest defect density levels studied.
- We confirmed previous measurements showing that there is no significant dependence of P_{MAX} upon defect density level before accelerated testing; in these tests we found that there is also no such dependence ***after*** accelerated testing.
- There is, however, a statistically-significant dependence of P_{MAX} upon defect density level at reduced insolation levels. The initial dependence increases with accelerated testing performed with Forward Bias, or with Light Soaking.
- We don't know whether this reduction in P_{MAX} at reduced light levels is related to Staebler-Wronski degradation; if so, we have identified a ***very small*** component in this catch-all phenomenon; if not, we have no certainty that this effect is stabilized after 800 hours; on the other hand, it appears to be ameliorated by high temperatures.
- We recommended new cell line measurement criterion that would increase cell line yield by 4% to 8%. The new criterion was adopted by USO.

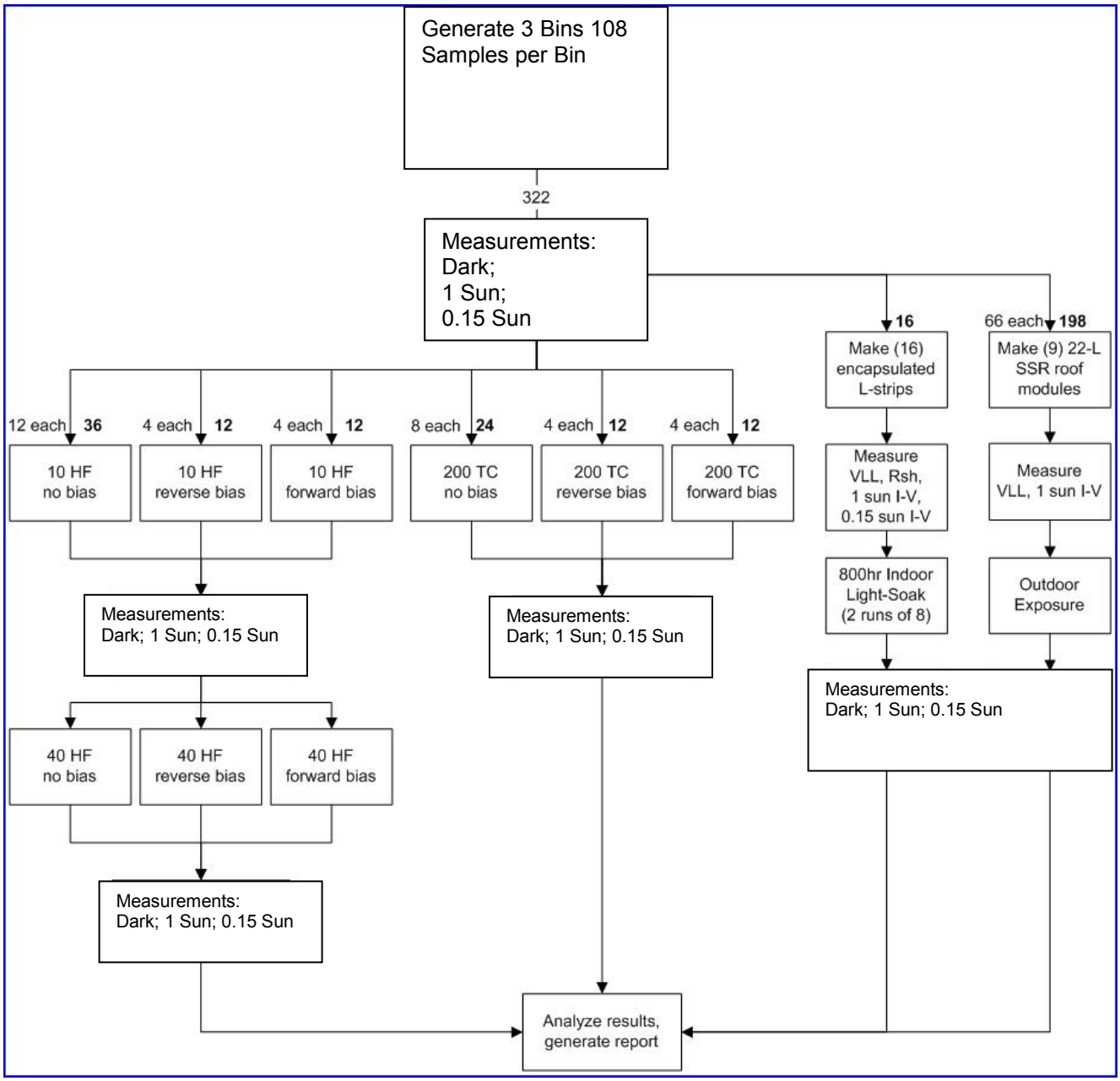

Fig. 4.3. Experimental procedure for testing and evaluating cells and modules as a function of defect density.

4.4.1 Initial Measurements (prior to accelerated testing) – Principal Findings

Effect of Defect Density on Cell Power (Initial Measurements)

At AM 1.5 there was no statistically significant correlation between P_{MAX} and defect density as shown in Fig. 4.4, consistent with previous findings.

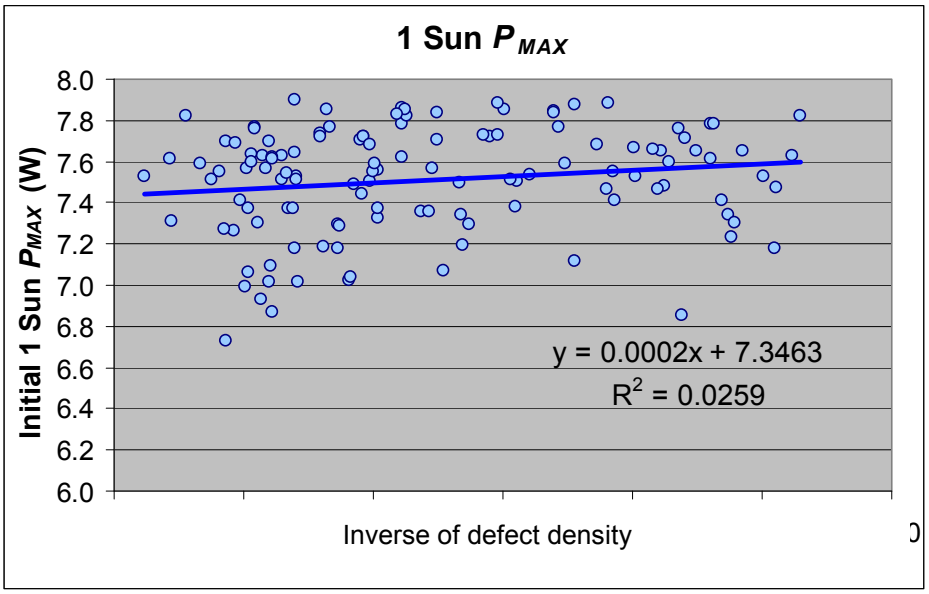

Fig. 4.4. P_{MAX} as a function of Cell Line defect measurement level.

There was, however, a significant correlation between P_{MAX} at lower light levels and defect density as shown in Figs. 4.5-6. The cells were measured in the Spire and neutral density filters used to attenuate the light level; the average of the J_{SC} measurement for all the cells was used as a measurement of the light intensity and to normalize P_{MAX}. The first-order effect is a reduction in normalized power with reduced light intensity independent of defect density level; the second-order effect is a further reduction with increasing defect density.

At the time we made these measurements we had some questions about accuracy of the pulsed-Spire measurements at reduced light intensity due to the increased charging-time of the cell at reduced levels of insolation. We have since looked at this in more detail and now know that our suspicions were correct and that the pulsed Spire measurements exaggerate (or create) the fall-off of P_{MAX} with reduced levels of insolation. This is discussed in section 3.2.1.a.

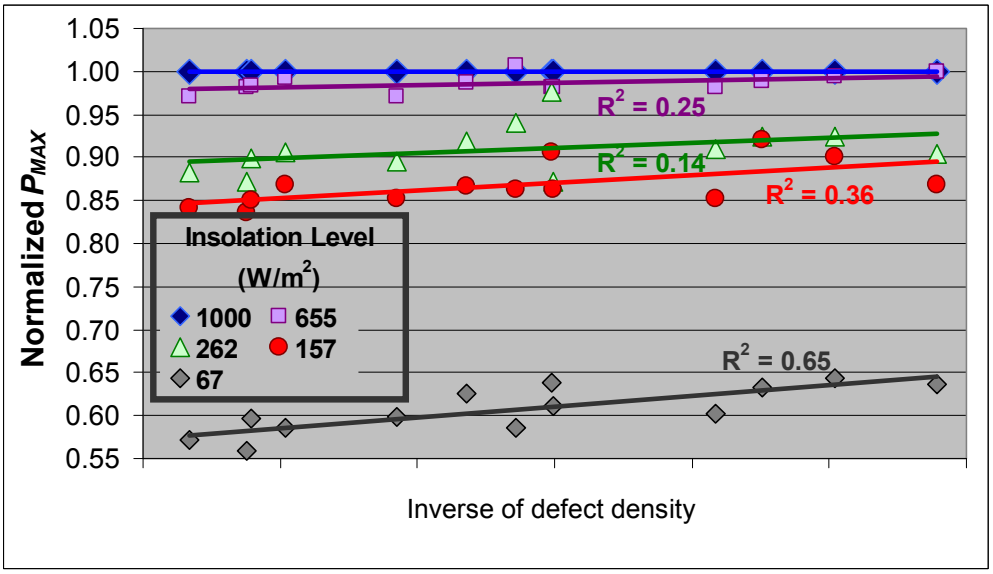

Fig. 4.5. P_{MAX} as a function of defect density for different levels of insolation.

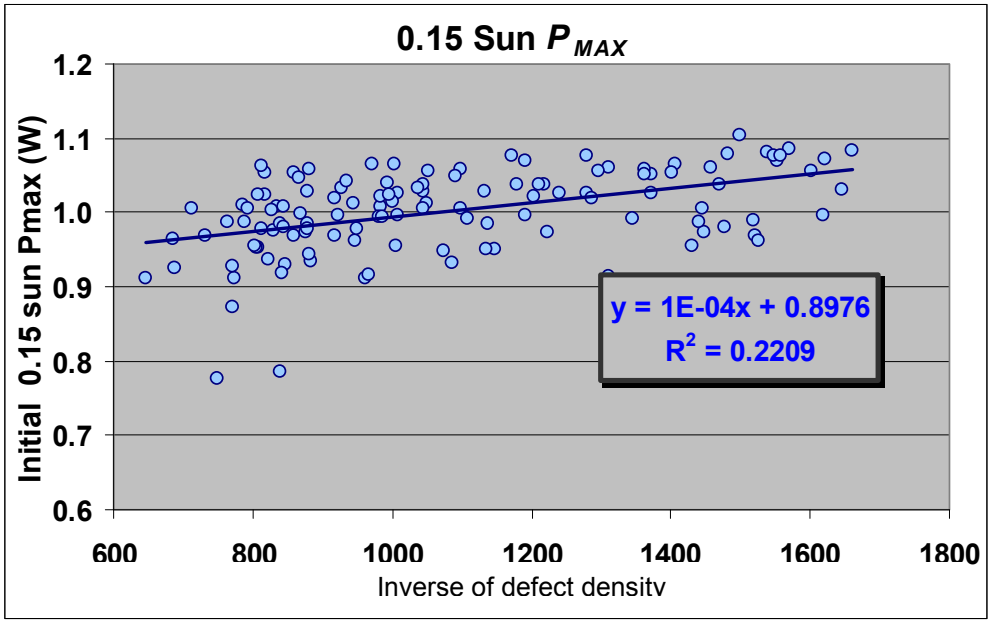

Fig. 4.6 Initial P_{MAX} as a function of defect density at 15% of AM 1.5 for all cells used in this study.

4.4.2 Final Measurements (after accelerated testing) – Principal Findings

Humidity-Freeze (HF) and Thermal Cycling (TC)

- With no bias, the dark R_{SHUNT} of the cells improved, though more so for HF than for TC (Fig. 4.7). After HF, all dependence of $P_{MAX,\ AM\ 1.5}$ and $P_{MAX,\ 15\%}$ upon initial defect density measurement disappeared; for TC there was no significant change (Figs. 4.8-9).

The HF tests spend about 10 X as long at high temperatures, and consequently we expect more annealing.

- With reverse bias, there were no statistically-significant trends.
- With forward bias, thermal cycling increased the reduction in $P_{MAX,\ 15\%}$ with increasing defect density (***ANOVA*** p-value of 0.003).

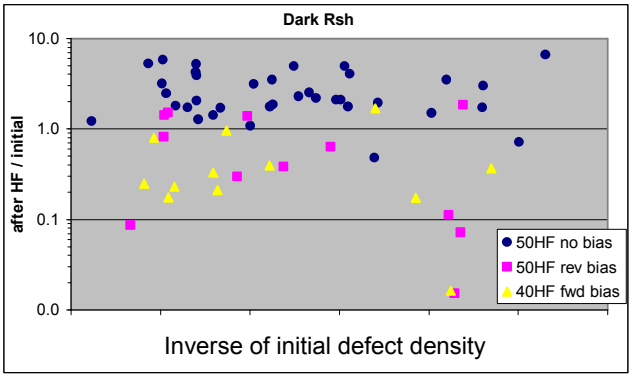

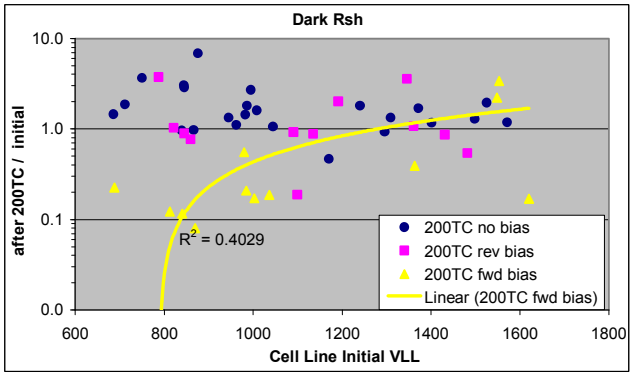

Fig. 4.7. Change in $R_{Shunt,\ Dark}$ after HF and TC.

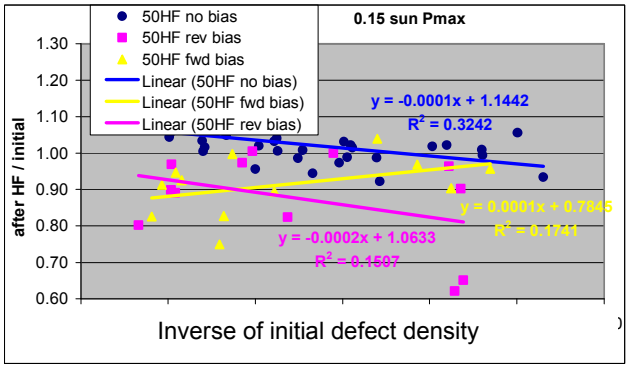

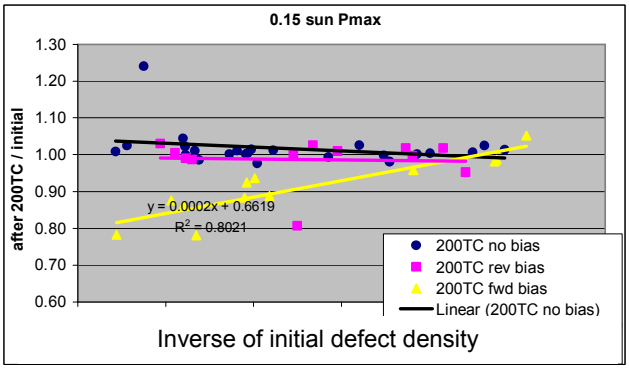

Fig. 4.8. Change in $P_{Max,\ 15\%}$ after HF and TC.

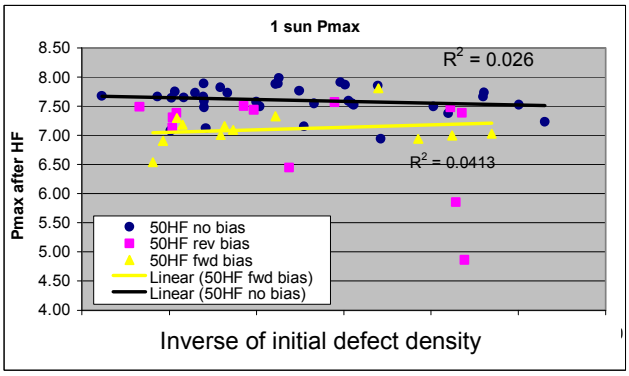

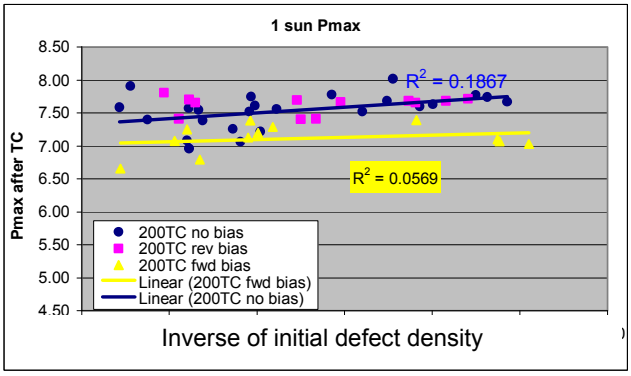

Fig. 4.9. Change in $P_{Max,AM\ 1.5}$ after HF and TC.

4.4.3 Light Soak Tests

At AM 1.5 the cells degraded by about 12%, with no correlation with initial defect density as shown in Fig. 4.10.

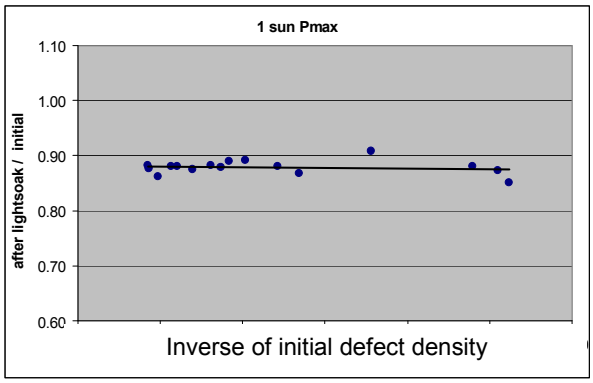

Fig. 4.10. Change in $P_{AM\ 1.5}$ after Light Soaking.

At 15% of AM 1.5 light intensity, the dependence upon P_{MAX} with defect density increased as it did with the forward-biased TC test samples (Fig. 4.11).

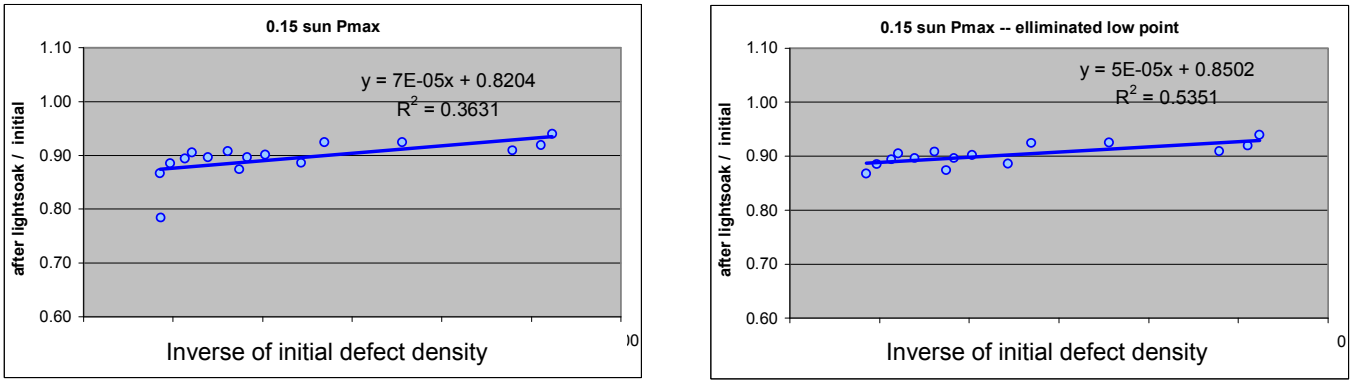

Fig. 4.11. Change in $P_{Max,\ 15\%}$ after Light Soaking.

The reduction in P_{MAX} as a function of light intensity and initial defect density measurement were used in a model that fit the reduction in P_{MAX} to defect density measurement and light intensity. We then used 5-minute period data over a 3 month period from the optical pyrometer on the NAHB Townhouse to calculate the effect on integrated power. We found a very slight reduction in integrated power for increasing defect density, though we suspect the pulsed Spire measurement overestimates the drop in normalized device efficiency with decreasing insolation level.

4.5 Results of Outdoor Testing

Figure 4.12 shows the relative measured power (P_{MAX}/Insolationout/constant or relative efficiency) of these modules 4 days after installation in the spring of 2005. We see the normalized power [Power/Insolation] first increase as the insolation decreases due to the series resistance in the circuit, and then decrease for smaller values of insolation. This decrease is clearly related to the defect density and modules with higher defect levels are more affected as the insolation level is decreased.

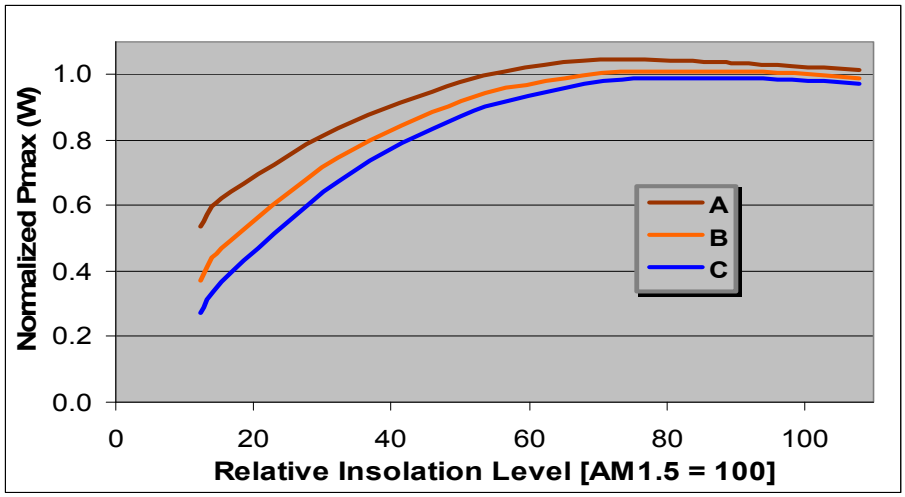

Fig. 4.12. Outdoor relative power output vs. insolation level for the average of the 3 modules in each bin. The modules were measured 4 days after installation. Bin A has the lowest defect density [standard], and Bin C has the largest defect density.

What was of greatest interest to us was how this pattern changed after a year of outdoor exposure. The perhaps surprising results are shown in Fig. 4.13 where the module power has been normalized to the power of the modules in Bin A. We see that after time, the effects associated with defects on the module power output have decreased.

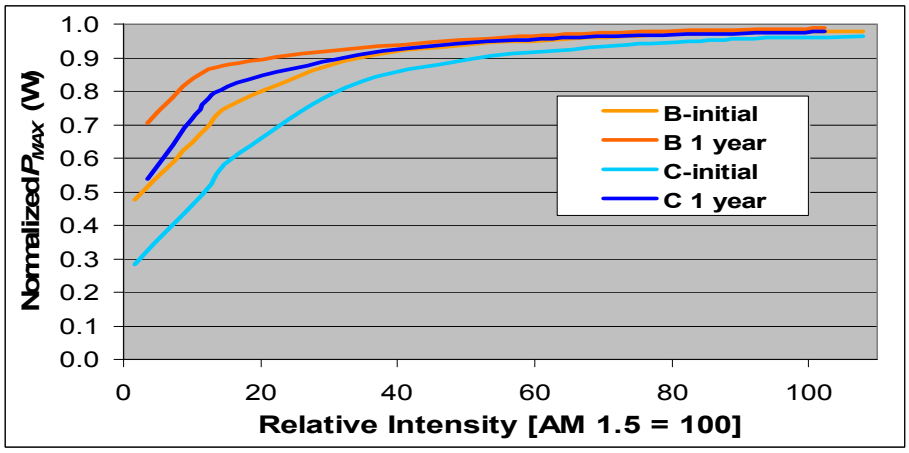

Fig. 4.13 Outdoor relative power/insolation vs. insolation level for the average of the 3 modules in each bin after 1 year outdoor exposure normalized to the average of the Bin A modules.

Since the data in Fig. 4.14 that show an improvement after exposure are relative to the Bin A data, a question that immediately comes to mind is whether the Bin B and Bin C modules improved, or the Bin A modules degraded. In Fig. 5 we have removed the normalization to the Bin A modules. We observe a roughly 15% reduction in P_{MAX} after stabilization (roughly inline with what we expect for a springtime measurement prior to annealing), and see that the effect of the defects at low light levels on P_{MAX} has indeed decreased.

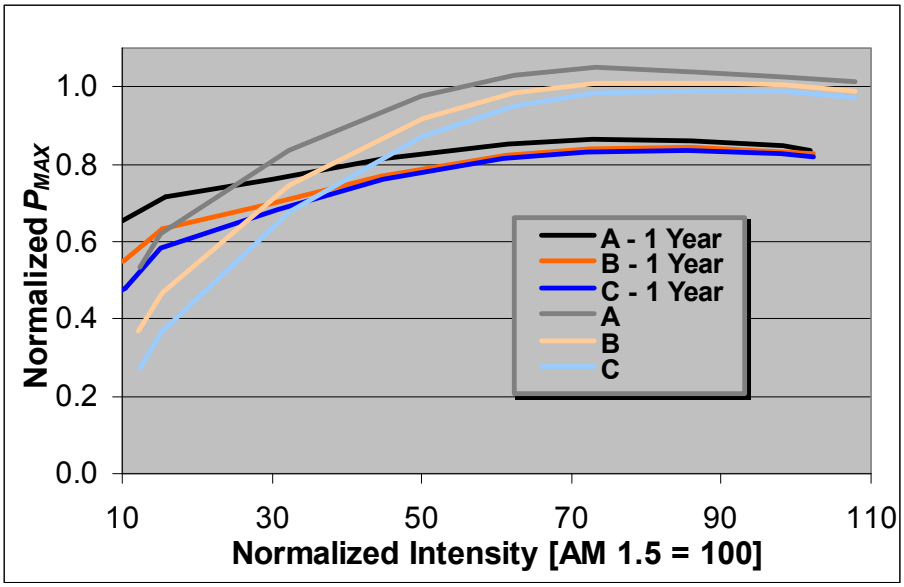

Fig. 4.14. Same data as in Fig. 4, but with normalization to the Bin A modules.

Future Work

These data need more careful analysis.

We shall continue to monitor these modules over time to see whether this trend continues, or stabilizes.

We previously used our indoor measurements of the reduction in P_{MAX} as a function of light intensity and initial defect density measurement in a model using 5-minute period insolation data over a 3 month period from the optical pyrometer on the NAHB Townhouse to calculate the effect of the defect density on the integrated power. We found a very slight reduction in integrated power for increasing defect density, though we suspected that the pulsed Spire measurement overestimated the drop in normalized device efficiency with decreasing insolation level. We shall now use these data to update our model.

These measurements provide more confirmation in our new cell line defect level sorting criterion.

REPORT DOCUMENTATION PAGE

Form Approved
OMB No. 0704-0188

PLEASE DO NOT RETURN YOUR FORM TO THE ABOVE ORGANIZATION.

1. REPORT DATE *(DD-MM-YYYY)*	2. REPORT TYPE	3. DATES COVERED *(From - To)*
May 2007	Subcontractor Report	23 April 2003 – 30 September 2006

4. TITLE AND SUBTITLE
Implementation of a Comprehensive On-Line Closed-Loop Diagnostic System for Roll-to-Roll Amorphous Silicon Solar Cell Production: Final Subcontract Report, 23 April 2003 – 30 September 2006

5a. CONTRACT NUMBER
DE-AC36-99-GO10337

5b. GRANT NUMBER

5c. PROGRAM ELEMENT NUMBER

6. AUTHOR(S)
T. Ellison

5d. PROJECT NUMBER
NREL/SR-520-41560

5e. TASK NUMBER
PVB56101

5f. WORK UNIT NUMBER

7. PERFORMING ORGANIZATION NAME(S) AND ADDRESS(ES)
Energy Conversion Devices, Inc.
1621 Northwood
Troy, Michigan 48084

8. PERFORMING ORGANIZATION REPORT NUMBER
ZDO-0-30628-11

9. SPONSORING/MONITORING AGENCY NAME(S) AND ADDRESS(ES)
National Renewable Energy Laboratory
1617 Cole Blvd.
Golden, CO 80401-3393

10. SPONSOR/MONITOR'S ACRONYM(S)
NREL

11. SPONSORING/MONITORING AGENCY REPORT NUMBER
NREL/SR-520-41560

12. DISTRIBUTION AVAILABILITY STATEMENT
National Technical Information Service
U.S. Department of Commerce
5285 Port Royal Road
Springfield, VA 22161

13. SUPPLEMENTARY NOTES
NREL Technical Monitor: Richard Mitchell

14. ABSTRACT *(Maximum 200 Words):* This report summarizes Energy Conversion Devices' diagnostic systems that were developed in this program, as well as ECD's other major accomplishments. This report concentrates on work carried out in the final (third) phase of this program, beginning in the fall of 2004 and ending in the fall of 2006. ECD has developed a comprehensive *in-situ* diagnostic system that: Reduces the time between deposition in the a-Si machine and device characterization from about 200 h to about 1 h; The Photovoltaic Capacitive Diagnostic systems measure the open-circuit voltage and charging rate (a measure of the short-circuit current) and intra-cell series resistance *for each cell* in the triple-junction device prior to deposition of the top conductive-oxide coating in a subsequent deposition machine. These systems operate with an rms precision of about 0.03% and have operated for almost 4 years with no need for servicing of the electronics or for calibration; Spectrometers are used to measure the ZnO thickness of the backreflector, a-Si thickness, and top conductive-oxide, coatings.

15. SUBJECT TERMS: PV; on-line closed-loop diagnostic system; amorphous silicon; solar cells; photovoltaic capacitive diagnostic (PVCD); open-circuit voltage; charging rate; short-circuit current; top conductive oxide coating; backreflector; triple-junction device;

16. SECURITY CLASSIFICATION OF:			17. LIMITATION OF ABSTRACT	18. NUMBER OF PAGES	19a. NAME OF RESPONSIBLE PERSON
a. REPORT	b. ABSTRACT	c. THIS PAGE			19b. TELEPHONE NUMBER (*Include area code*)
Unclassified	Unclassified	Unclassified	UL		

Standard Form 298 (Rev. 8/98)
Prescribed by ANSI Std. Z39.18